Magnesium-aluminum-zirconium oxide amorphous ternary composite: a dense and stable optical coating

ABSTRACT

In the present work, the process parameter dependent optical and structural properties of MgO-Al_2O_3-ZrO_2 ternary mixed-composite material have been investigated. Optical properties were derived from spectrophotometric measurements. The surface morphology, grain size distributions, crystallographic phases and process dependent material composition of films have been investigated through the use of Atomic Force Microscopy (AFM), X-ray diffraction analysis and Energy Dispersive X-ray (EDX) analysis. EDX analysis made evident the correlation between the optical constants and the process dependent compositions in the films. It is possible to achieve environmentally stable amorphous films with high packing density under certain optimized process conditions.

Key Words: Optical coatings, thin films, mixed-composite-films, zirconium dioxide, magnesium oxide, aluminum oxide, inhomogeneity, atomic force microscopy, surface roughness, optical constants, X-ray diffraction, EDX-analysis, solid solution.

Information Page

Magnesium-aluminum-zirconium oxide amorphous ternary composite: a dense and stable optical coating

By

N. K. Sahoo* and A. P. Shapiro
NASA/ George C. Marshall Space Flight Center
Mail Code: EB52, Huntsville, AL 35812

Address for Correspondence:
A. P. Shapiro
NASA/George C. Marshall Space Flight Center
Mail Code: EB52, Huntsville, AL 35812
E-mail: alan.shapiro@msfc.nasa.gov

1.	Information Page	: 1page
2.	Title Page	: 1page
3.	Abstract	: 1page
4.	Text	: 12pages
5.	References	: 3pages
6.	Caption to Tables	: 1page
7.	Caption to Figures	: 3pages
8.	Tables	: 2
9.	Figures	: 25

10. Manuscript with items 1 to 9 (original figures and tables) and four copies are enclosed.

---

*Permanent Address: Spectroscopy Division, BARC, Bombay-40085, India.

Title Page

Magnesium-aluminum-zirconium oxide amorphous ternary composite: a dense and stable optical coating

By

N. K. Sahoo* and A. P. Shapiro
NASA/ George C. Marshall Space Flight Center
Mail Code: EB52,
MSFC, Huntsville, AL 35812

*Permanent Address: Spectroscopy Division, BARC, Bombay-40085, India

Magnesium-aluminum-zirconium oxide amorphous ternary composite: a dense and stable optical coating

ABSTRACT

In the present work, the process parameter dependent optical and structural properties of MgO-Al_2O_3-ZrO_2 ternary mixed-composite material have been investigated. Optical properties were derived from spectrophotometric measurements. The surface morphology, grain size distributions, crystallographic phases and process dependent material composition of films have been investigated through the use of Atomic Force Microscopy (AFM), X-ray diffraction analysis and Energy Dispersive X-ray (EDX) analysis. EDX analysis made evident the correlation between the optical constants and the process dependent compositions in the films. It is possible to achieve environmentally stable amorphous films with high packing density under certain optimized process conditions.

Key Words: Optical coatings, thin films, mixed-composite-films, zirconium dioxide, magnesium oxide, aluminum oxide, inhomogeneity, atomic force microscopy, surface roughness, optical constants, X-ray diffraction, EDX-analysis, solid solution.

Magnesium-aluminum-zirconium oxide amorphous ternary composite: a dense and stable optical coating

1. Introduction

The post-deposition instability of conventional physical-vapor-deposited, refractory-oxide-thin-films has persisted as a major obstacle in optical coating technology.[1] Precision filters which make use of such films suffer from water vapor induced spectral shift. In typical electron beam deposited coatings, the root cause of this undesirable feature is columnar growth structure.[1-3] This structure contains void distributions and grain boundaries which allow water vapor to adsorb and desorb from the film leading to substantial instabilities in optical and mechanical properties. One of the possible approaches to eliminate such a growth condition is to provide more kinetic energy to the vapor molecules. This leads to greater mobility during the condensation process thereby leading to higher packing density.[1,4] Alternately, one may mix several materials in the vapor state to achieve similar results.[5] Among the various film growth structures, it is always preferable to have a amorphous (or glassy) film structure for better stability and improved optical properties as opposed to the usual polycrystalline or very rare crystalline structures.[6,7] The amorphous structure is also important in reducing the bulk scattering losses in the films.[6] Over the years, such growth conditions have been achieved by various advanced techniques which include reactive sputtering, ion beam sputtering (IBS), plasma ion-assisted deposition, etc.[8-11] Such techniques are quite complex and some times difficult to implement for the non-quarterwave coating design. In recent years, composite films are gaining the attention of researchers attempting to develop more stable optical coatings. It has been already established that it is possible to achieve novel film properties by mixing various thin film materials either during the vapor stage or as a solid solution.[12] Since co-deposition techniques require very high quality process calibration and control, composite materials in solid solutions are favorable because of the simplified deposition process.[12,13] It has been reported by various investigators that it is possible to stabilize the tetragonal or cubic phase in ZrO_2 by adding various other refractory oxides which include MgO, CaO, Al_2O_3, Y_2O_3, etc.[14] Some of the binary composites have excellent process modulated index tunability. Our earlier work on ZrO_2MgO binary system has shown a very interesting oxygen dependent refractive index tunability for the films deposited from the solid solution.[12] The majority of earlier reports on other partially stabilized binary systems have reported polycrystalline film structures.[15] So far, a very limited amount work has been

performed on ternary composite systems. In the present work, we have carried out extensive investigations on MgO-Al_2O_3-ZrO_2 ternary system and optimized the process to highly stable optical coatings. Interestingly, it has been observed that cubic structure typical to ZrO_2MgO system has been completely eliminated by adding the third component Al_2O_3 to the solid solution. The films evaporated from the ternary composite have a highly amorphous structure, which is the most preferable growth condition for high spectral quality and environmentally stable optical coatings.

2. Earlier Research on Partial Stabilized Zirconia Films

Historically, Zirconia (ZrO_2) has played a very important role in optical coating technology because of its superior properties such as high refractive index, high melting temperature, hardness, low thermal conductivity, better corrosion resistance, extended spectral transmission, better compatibility with SiO_2 and stability for high power laser applications.[14,16-17] The polymorphic nature of ZrO_2 is very well known and has been the subject of many studies. Partially stabilized zirconias (PSZ's) are mostly two-phase ceramics that have optical and mechanical properties generally superior to those of fully stabilized bodies. The main advantage of PSZ over fully stabilized zirconia is its low overall thermal expansion coefficient.[18,19] It is possible to stabilize the tetragonal, monoclinic or cubic phase in the material by adding suitable quantities of various other refractory oxides to zirconia which include MgO, In_2O_3, Y_2O_3, CaO, Al_2O_3, Sc_2O_3, SnO_2, ZnO, CeO, etc. Very interestingly, some of these refractory oxides have exhibited extended solid solubility in ZrO_2 yielding very different optical and structural properties.[12] A variety of structural symmetries can be achieved through the addition different amounts of stabilizing solutes to the ZrO_2 host. It has been reported by Qadri and coworkers that the cubic phase can be conveniently achieved in electron beam co-evaporated zirconia-zincia thin films.[14] Gilmore and his coworker reported achieving the tetragonal phase in magnetron sputtered ZrO_2-Al_2O_3 films.[20] Tsai and co-worker reported that the off-axis grown yttria-stabilized-zirconia (YSZ) films exhibit atomically smooth interfaces.[15] It is generally accepted, however, that the most useful mechanical properties are obtained by partial stabilization so that, most frequently, a two or three-phase microstructure results. During earlier investigations, experimenters reported that the improved properties in partially stabilized zirconia (PSZ) materials were due to the simultaneous presence of both monoclinic and cubic structures. Subsequently it was reported that it is possible to achieve a room temperature stable tetragonal phase by adding a suitable amount of CaO to zirconia.[18] Although the results on binary mixtures are very interesting and benefited number of technological programs, not much work

has been performed with ternary mixtures. There are a few reports available on zirconia-magnesia-ceria ternary compositions. Ruff and co-workers have reported some results on ZrO_2-ThO_2-CaO, ZrO_2-ThO_2-MgO, ZrO_2-BeO-CaO and ZrO_2-BeO-CeO_2 ternary systems.[21-22] On the basis of the results presented in these experiments, it is observed that the melting point of zirconia can be lowered by addition of the third component CeO_2. So far no investigations have been carried out on optical and physical properties of ternary systems. In the present study we have investigated optical and structural properties of a very interesting ternary composite, MgO-Al_2O_3-ZrO_2, evaporated from a solid solution. Earlier investigations report that zirconia can be stabilized to a cubic phase with the addition of MgO, where as the addition of Al_2O_3 leads to tetragonal phase.[20] During the present investigation, we have observed that, when both Al_2O_3 and MgO are present in the composite, both of the above phases disappear leading to most desirable amorphous condition. Very interesting non-linear optical and structural inhomogeneities have been observed in films deposited under various deposition conditions. It is also possible to obtain very high packing density in the composite leading to practically negligible air-to-vacuum shift in the spectral characteristics of the coatings.

3. Experimental Details

The Balzers BAK-760 coating system, optical monitor, and other analytical equipment used for this experiment has been described elsewhere in detail.[12] We deposited ternary composite films on 25-mm-diameter, 3- to 5- mm-thick optically polished quartz and BK7 substrates by evaporating optical grade MgO-Al_2O_3-ZrO_2 solid solution typically 99.0% pure (M/s CERAC Inc., supplied, stock number M-1126). A total of over twenty samples deposited under various process conditions were prepared for the present optimization study. When a particular parameter was varied, the other parameters were kept constant at an optimum value to observe the distinct changes in the optical and structural properties of the film. Energy Dispersive X-ray (EDX) analysis confirmed the presence of a trace amount of Ca in some of the thin film samples. During e-beam evaporation from a crucible, this material has a tendency to form towering structures of 1-2" in height that somewhat resemble stalagmites. One has to take necessary precaution while using multi-crucible sources for the deposition because such growths may obstruct the crucible rotation while switching between the materials. Careful pre-conditioning designed to initially obtain a level, uniform melt sometimes reduces this undesirable behavior. During this investigation, the pre- and post-deposition transmittance and reflectance spectra of the films were recorded with the

BALZERS GSM-420 broadband, optical monitor/controller over 350-975nm. Post-deposition spectral characteristics over an extended wavelength region (200-2000nm) were recorded using a Perkin-Elmer Lamda-19 UV-vis-NIR spectrophotometer. The mean optical constants were derived by use of "*SPECTR*" software developed by Sahoo.[12] This software has a special provision to draw the computer generated envelopes for the transmittance and reflectance extrema even for the films that have highly non-linear inhomogeneity.[23,24] The semi-quantitative process dependent compositions of the films were determined by EDX analysis. The Surface morphologies of selected coatings were investigated using Scanning electron microscopy (SEM). Surface topography, bearing ratio and power spectral densities of coatings were analyzed using a Topometrix TMX 2000 series atomic force microscope. Structural properties of the films were investigated using X-ray diffraction analysis carried out on Rigaku (USA) diffractometer system.

4. Films with Non-linear and Mixed Inhomogeneity

It has been observed during online spectral monitoring of the films under certain deposition condition that index of refraction varied continuously along the growth direction in several non-linear fashions. Such non-linear and mixed inhomogeneities have very interesting effects on overall spectral characteristics of the coatings. We have already discussed these effects in our earlier investigations on ZrO_2MgO binary system.[12] Most recently, an extensive theoretical analysis has been published by Tikhanravov et al., on influences of mixed inhomogeneities on the spectral characteristics of single thin films.[25] It is interesting to note that the transmittance and reflectance extrema in films of this type show considerable modulation which is very different than in films with linear inhomogeneity. In linear inhomogeneity, the change in spectral amplitude becomes more prominent for the wavelengths that satisfy the relationship:[25]

$$\lambda_m = \frac{2.n.z_d}{m} \qquad m=1,2,3\ldots\ldots, \tag{1}$$

where the various notations in this equation are as per the reference-25. In case $n>n_s>n_a$, the wavelengths λ_m corresponds to transmittance maxima (reflectance minima). In films with non-linear inhomogeneity, the interference extrema modulation depends on the extent and quality of the non-linear growth. For a weakly absorbing dielectric film with a functional index inhomogeneity of $\tilde{n}(z)$, the modulation in reflectance and transmittance amplitudes at normal incidence are given by the following analytical expressions:

$$\delta R(\lambda) = -\frac{4.\pi.n}{\lambda.n_s} T(\lambda) \int_0^{z_s} \mathrm{Im}\left[r'(\lambda) \left(\cos\frac{2\pi nz}{\lambda} + i.\frac{n_s}{n} \sin\frac{2\pi nz}{\lambda} \right)^2 .\tilde{n}(z) \right] dz \ , \qquad (2)$$

and

$$\delta T(\lambda) = -\delta R(\lambda) + \frac{4.\pi.n}{\lambda.n_s} T(\lambda) \int_0^{z_s} \left(\cos\frac{2\pi nz}{\lambda} + i\frac{n_s}{n} \sin\frac{2\pi nz}{\lambda} \right)^2 \mathrm{Im}[\tilde{n}(z)] dz \ , \qquad (3)$$

where the various terms have their meanings as per the reference-25. If the function $\tilde{n}(z)$ is smooth so that its derivatives, including higher order terms, can be neglected, then the above expressions can be assessed more conveniently. In case of highly non-linear index functions, the computation of amplitudes of spectral modulation is very complex. These expressions also can be used for films with mixed modes of inhomogeneity (i.e. mixture of both homogeneous and inhomogeneous growth profiles). These mixed inhomogeneities are very frequently observed in composite films.[12]

In case of our present studies, we observed the most intense modulation to be in weakly absorbing region of the spectra (i.e. near-UV and UV region). The derivation of optical constants for such films from spectrophotometric measurements alone is extremely difficult. Sometimes numerical modeling helps in getting a starting solution for the computation. Fortunately the interference peak positions are very weakly affected by changes in index inhomogeneities.[26,27] As a result, it is possible to compute the mean refractive index from the order of the peaks, peak positions and physical thickness as described by our earlier work. In such case, information from quartz crystal data, on-line optical monitoring values and thickness of the films measured by an independent technique appreciably improves the computational accuracy. Also, it is known that for a film with small inhomogeneity, the best fit with a homogeneous film model is obtained with a refractive index that is close to the geometrical mean of the refractive index values at the physical boundaries (i.e. the top and bottom) of the inhomogeneous film.[25] Computation of mean optical constants for non-linear inhomogeneous films has been discussed extensively in our earlier work on ZrO_2MgO binary composite films.[12] The same procedure has been adopted to derive optical constants of the present ternary films. The modulated experimental reflectance and transmittance of two non-linear inhomogeneous films have been depicted in Fig. 1 and Fig. 2. It is also observed that it is possible to obtain fairly homogeneous growth structure under ambient as well as higher substrate temperature as shown in Fig.3. It is observed that the mean refractive indexes of the films (n_m) follow a four-parameter Cauchy dispersion equation as follows:

$$n_m(\lambda) = a_1 + \frac{a_2}{\lambda^2} + \frac{a_3}{\lambda^3} + \frac{a_4}{\lambda^4} \ , \qquad (4)$$

where a_1, a_2, a_3 and a_4 are the coefficients for fitting. In Table-1, Cauchy coefficients for the films deposited under various substrate temperature (same rate and oxygen pressure) have been presented. The mean extinction coefficients (k_m) of these films follow a four-parameter logistic dispersion equation as follows:

$$k_m(\lambda) = \frac{a}{\left[1+\left(\lambda/c\right)^b\right]^d} \quad . \tag{5}$$

In this equation, the parameter a is the asymptotic maximum, b is the slope parameter, c is the value at inflexion point of the curve and d is a symmetry parameter. The values of the coefficients for the films deposited under varying substrate temperature are given in Table-2.

5. Effect of Substrate Temperature

Substrate temperature has a very prominent effect on optical constants as well as structural properties in this composite. The films grown under ambient conditions show a fairly homogeneous growth structure. It is worth mentioning that even at ambient conditions the films have very high packing densities. The pre- and post-deposition transmittance characteristic of one such film is depicted in Fig. 4, where it can easily be seen that there is infinitesimal air-to-vacuum shift. The films are fairly homogeneous at the two extreme experimental temperatures as shown in Fig. 3. The rates and oxygen pressures were maintained at 0.4 nm/s and base pressure, respectively, as the substrate temperature was varied. At all other temperatures, non-linear inhomogeneity was the dominant growth structure and this is evident in the transmittance and reflectance spectra. In Fig. 1 and Fig. 2, such a behavior is depicted for two different substrate temperatures and oxygen pressures. The films grown at ambient temperature have the minimum index as shown in Fig. 5. When the substrate temperature was increased from ambient to 125 °C, the corresponding refractive index increased from 1.68 to ~1.86 @ λ=600nm and then decreased to 1.78 with the further increase of temperature to 175 °C. When the temperature is increased beyond 175 °C, the refractive index value improved and it approached saturation above 237 °C. This interesting behavior is most likely due to temperature dependent compositional changes in the films, which are clearly evident in the EDX analysis. The mean extinction coefficients also have shown a similar behavior. There is a remarkable improvement in these coefficients in the temperature ranges between 150 to 200 °C as shown in Fig. 6.

Excluding the dip in the curve, the variation in refractive index as a function of substrate temperature approximately follows the trend one might expect for

conventional dielectrics. Typically, the refractive index monotonically improves as temperature increases, up to an optimal value, due to higher mobility that leads to better packing density and improved order in the film.[1] Extinction coefficients typically improve with higher substrate temperatures, once again up to a limiting maximum temperature. Crystallographic, structural, and compositional changes, however, may alter the conventional trends.

6. Effect of Rate of Evaporation

Rate has a very distinct influence on optical constants as well as structural properties of the composite films under present investigation. As it is well known, the amount of kinetic energy that the vapor atoms carry after leaving the source is dependent upon the rate of deposition.[16] This influences the mobility of the atoms during nucleation and growth of the films on the substrate. During the rate variation, the substrates' temperatures and oxygen pressures were maintained constant at 162 °C and $1x10^{-4}$ mbar respectively. It is observed that the rate of evaporation has an optimum value that leads to the improved and favorable optical constants. We found this value to be 1 nm/s for our present set of conditions. Further increases in the rate deteriorated the index value appreciably, as shown in the Fig. 7. Similar trend was also observed for the mean extinction coefficients. The extinction coefficient values became higher for the films deposited rate more than 1nm/s, as depicted in Fig. 8. Such behavior can be attributed to various compositional changes that occur due to the dynamics of the nucleation and growth process under different rates of deposition.

In conventional films, both refractive indices typically improve monotonically to optimum values (higher refractive index and lower extinction coefficient) as rate increases to an optimum value due to improved vapor energy and mobility. Beyond an optimum rate, incomplete relaxation occurs along with trapping of gases in voids leading to decreased index and higher roughness.[1] In the present ternary films, the refractive index follows this trend, whereas the extinction coefficient remains consistently low except at the fastest rate.

7. Effect of Oxygen Pressure

Oxygen pressure also has a very pronounced effect on the films growth conditions. During variation of oxygen pressure, the substrates' temperatures and deposition rates were maintained at 162 °C and 0.4 nm/s respectively. The optical constants showed an optimum value for the films deposited at $5x10^{-5}$ mbar as shown in

the Fig. 9. On both side of this value the index shows a downward trend. The slope for mean refractive index above $3x10^{-4}$ mbar is steeper compared to that of lower oxygen values. It is interesting to note that the oxygen enrichment factor is not as high as in the case of binary composites.[28] The extinction coefficients increase in value at higher oxygen pressure, especially for the films deposited above $3x10^{-4}$ mbar as depicted in Fig. 10. It is interesting to note from the EDX results that relative amount of Zr in the films became higher than Al at higher oxygen pressures above $6x10^{-4}$ mbar. This might be due to a relatively longer mean free path for the higher atomic mass Zr material in the oxygen or perhaps to a superior accommodation coefficient of Zr under higher oxygen pressure.[12]

With reactive evaporation of most dielectric oxides, both refractive indices typically improve monotonically to optimum values (higher refractive index and lower extinction coefficient) as oxygen pressure increases to an optimum value due to improved oxidation of the film materials.[1] Beyond an optimum pressure, the energy of impinging material declines as the mean free path declines. In addition, excessive trapping of gases in voids occurs. Once again these effects lead to decreased index and higher roughness. In the present ternary films, the refractive index follows this trend, whereas the extinction coefficient remains consistently low except at the higher pressures.

8. Atomic Force Microscope (AFM) Analysis

We have used atomic force microscopy to investigate the surface topography both qualitatively and quantitatively. The equipment used for this investigation is a Topometrix TMX 2000 series Explorer AFM. The probes used for the scans are the standard triangular cantilever types (AFM tips-1520) with a typical spring constant of 0.032 N/m. The surface morphology of a film deposited with a substrate temperature of 162 °C, deposition rate of 1 nm/s and oxygen pressure of $2x10^{-4}$ mbar is depicted in Fig. 11. The power spectral density (PSD) function resulting from topographic measurements provide much qualitative information on the surface profile and grain structure in thin films. It is well known in topographic analysis that the roughness is proportional to the area under the curve for each PSD plot.[29] The evolution of roughness can be very well described based on the transitions in PSD plots. The statistical PSD function ($P(k)$) is defined as the square of the magnitude of the Fourier transform of the surface profile; it provides pertinent information concerning the

amplitude of the surface features as a function of lateral spatial frequency. From a line height profile $Z(x)$, the $P(k)$ function is derived as[30]

$$P(k) = \frac{1}{L}\left|\int dx . e^{i2\pi kx} . Z(x)\right|^2 \quad \text{in units of } \text{Å}^2\mu\text{m}, \tag{6}$$

where L is the scan length in μm, $Z(x)$ the line height profile in Å and k the spatial frequency in μm^{-1}. The bearing ratio, which is defined as the percentage of total data appearing above the selected Z-height, also helps in presenting the distribution of various sizes of grains in the sample. The temperature, rate and oxygen pressure dependent PSD function and bearing ratio (BR) plots are depicted in the Figs. 12-17. It can be seen from Fig. 12, that the grain size and surface roughness is the highest for the films deposited at a substrate temperature of 175 °C. The films deposited at highest substrate temperature have shown the lowest surface roughness as well as smaller grain size. But like refractive index plots, the temperature dependent roughness also has shown a very interesting modulative effect between 125-190 °C. The films deposited at both the highest and lowest rates of evaporation have shown higher roughness values as compared with intermediate rates of deposition. Films deposited between 0.6-1.0 nm/s have the minimum roughness, as shown in the Fig. 13. The films deposited under base pressure have smoother surface profiles that those deposited at high oxygen pressure, as depicted in the Fig. 14. Films deposited at $8x10^{-4}$ mbar have very high roughness values. Bearing ratio plots for the films deposited under different process parameters have been depicted in Figs. 15-17. The BR plot for the film deposited under our highest experimental oxygen pressure are most distinctive, indicative of a very rough surface.

9. X-ray Diffraction Analysis

X-ray diffraction measurements were carried out on a Rigaku (USA) diffractometer with $Cu(K_\alpha)$ (λ=1.5418 Å) radiation. The angular resolution was .02° for each sample. Since the films were deposited on quartz as well as BK7 substrates, the short-range order of SiO_2 contributes to the background structure, especially in the lower 2θ region. Diffraction spectra from most of the samples have shown completely amorphous structure. Films grown at higher deposition rates and lower oxygen pressure, however, show an extremely weak tetragonal phase as depicted in the Fig. 18. The films deposited at both ambient and at the highest experimental temperatures are the most completely amorphous, as shown in the Fig. 19. This characteristic is most likely due to the presence of higher relative quantities of Al_2O_3 in the sample. Earlier works by Glimore and co-worker on ZrO_2+Al_2O_3 composite have indicated amorphous

structure in their reactive magnetron sputtered films.[20] The phase diagram of zirconia and alumina has been reported to be of eutectic type with a very low solid phase solubility factor.[20] It is also reported that it is possible to convert the amorphous structures to a stable tetragonal phase with suitable post-annealing. Our experiments have shown that the rate of evaporation has more prominent effect on the crystallographic phase as compared to substrate temperature and oxygen pressure as shown in Fig. 18.

10. Compositional Analysis by Energy-Dispersive X-Ray (EDX)

In order to determine the cause of large variation in the optical constants in films prepared under varied deposition conditions, we tried to investigate the variation in composition in the samples. Other investigators have pointed out that the relative amounts of either Al_2O_3 or MgO in binary solution with ZrO_2 substantially affects the optical and structural properties. In order to measure the relative amount of Zr, Al, Mg and O_2 in our samples, we performed relative compositional analysis using the energy dispersive X-ray (EDX) feature available in a 4Pi Environmental Scanning Electron Microscope, model Spectral Engine-II. The electron beam energy used was 10 KeV with a Detector resolution of 145 eV. The carbon peak at 0.25KeV is the usual peak associated with hydrocarbon contamination nearly always present on samples introduced from the laboratory environments. Most of the films have shown the presence of a trace amount of Ca in the samples (also indicated by the supplier). A typical EDX spectrum, shown for the film deposited at substrate temperature of 188 °C, rate 0.4 nm/s and without additional oxygen, is depicted in Fig. 20. Comparisons between the material composition and optical constants in films deposited under varying process conditions reveal very interesting, but complex, relationships. The relative amount of Zr in the composite films varied drastically as a function of oxygen pressure in a non-systematic fashion as shown in Fig. 21. The lowest index occurs at the highest oxygen pressure where Zr content reaches a maximum; however, the lowest Zr content does not correspond to the highest index value. Regarding variations in composition as a function of deposition rate, the largest compositional variation occurs at the minimum deposition rate value of 4 nm/s (Fig. 22). At this value, the relative amount of Zr is drastically lower and Mg is slightly higher, whereas the index of refraction is rather low. At other deposition rate values, there is minimal variation in composition with moderate change in index. EDX analysis of the films deposited with various substrate temperatures (Fig. 23) have clearly indicated the relative increase in Zr content with the temperature except at our highest experimental temperature. There

is some complex modulation of the relative composition of Mg and O_2 as a function of temperature. Overall, it is difficult to establish any suitable functional dependence between the compositions and mean optical constants. This is, most probably, due to very complex growth structure of the ternary composite film involving four elements (Zr, Al, Mg and O_2) that are affected by the dynamics of the nucleation process on the substrate surface.

11. Metal Dielectric Spectral Selective Solar Filter

Using this composite material, we have been able to start development of a highly stable pre-filter coating for a solar vector magnetograph instrument. It is well known the most popular metals like Ag, Au and Al have better film properties when deposited under ambient conditions. Metallic films mostly carry a tensile stress.[31] When combined with dielectrics, one has to use a dielectric with compressive stress or very low tensile stress in order to develop stable multilayer metal-dielectric filters, especially when number of metal layers is high in the device. Most conventional dielectrics have very inferior optical properties when deposited under ambient conditions. Most of the time, the post-deposition behavior is very unstable in devices that make use of such dielectrics. The MgO-Al_2O_3-ZrO_2 ternary composite used in this study has excellent optical and mechanical properties even under ambient conditions. Because of overall low residual stress, it is an ideal material for developing metal-dielectric filter. The high packing density of the films even at ambient conditions makes the post-deposition spectral characteristic very stable as is evident in comparisons between the measurements in air and vacuum. In Figs. 24 and 25, we have shown the experimental spectral characteristics of two different developmental metal-dielectric filters measured in air as well as vacuum. The typical design for these filters (Fig. 25) is as follows:

Sub. (72.48T 15.77M 132.33T 15.55M 432.48T 14.66M 134.12T 23.93M 727.71T 13.03M 78.77T) Air,

where **T** is the ternary composite layer and **M** is the silver layer. All the design thicknesses are given in nm (physical thickness). Silver thicknesses in this design are constrained to remain more than a critical thickness in order to avoid island growth and the high stress regions.[32]

12. Conclusion

The process parameter dependent optical and structural properties of MgO-Al_2O_3-ZrO_2 ternary composite films have been investigated in detail. A highly stable, stress-free, amorphous structure has been achieved in these films ideal for development

of environmentally stable optical coatings. The stress-free feature has enabled development of stable, precision metal-dielectric multilayer filters. This composite also has very interesting non-linear inhomogeneous properties as is evident in the transmittance and reflectance spectra. It may be possible to make use of such behavior to develop rugate filters. It is also possible to achieve the homogeneous growth conditions, which can be utilized in development of conventional optical coatings. It is difficult at this point to establish a suitable functional dependence between various elementary compositions and optical properties of the ternary film. Such an understanding may be possible with more complex on-line analysis and modeling of the deposition-parameter-dependent-nucleation process in these films.

13. Acknowledgment

This research was performed while N.K. Sahoo held a National Research Council-NASA/Marshall Space Flight Center (MSFC) Research Associateship. The authors acknowledge the help of Marcus Vlasse of MSFC in carrying out the x-ray diffraction analysis and are also grateful to him for the useful technical discussions in interpreting the data. The authors also acknowledge the help of J.E. Coston of MSFC in performing EDX and SEM analysis.

14. References

1. H.K. Pulker and K.H. Guenther, "Reactive physical vapor deposition processes", in Thin Films for Optical Systems, F. R. Flory ed. (Marcel Dekker Inc., New York, 1995), Chap. 4, p. 91-115.
2. M. Harris, H.A. Macleod, S. Ogura, E. Pelletier and B. Vidal, "The relationship between optical inhomogeneity and film structure," Thin Solid Films **57**, 173-178 (1979)
3. S. Ogura, "Dynamic characteristics in optically inhomogeneous films," in Thin Films for optical systems, K.H. Guenther ed., Proc. SPIE **1782**, 377-388 (1992)
4. P.J. Martin, R.P. Netterfield and W.G. Sainty, "Modification of the optical and structural properties of dielectric ZrO_2 films by ion-assisted deposition," J. Appl. Phys. **55**, 235-241 (1984)
5. D.M. Sanders, E.N. Farabaugh and W.K. Haller, "Glassy optical coatings by multi-source evaporation", in Thin Film Technologies and Special Applications, W.R. Hunter, ed., Proc. SPIE **346**, 31-38 (1982)
6. Jyh-Shin Chen, Shiuh Chao, Jian-Shiun Kao, Huan Niu and Chih-Hsin Chen, "Mixed films of TiO_2-SiO_2 deposited by double electron beam coevaporation", Appl. Opt. **35**, 90-96 (1996)
7. Y. tsou and F.C. Ho, "Optical properties of hafnia and coevaporated hafnia:magnesium fluoride films", Appl. Opt. 35, 5091-5094 (1996)
8. Rung-Ywan Tsai, Mu-Yi Hua and Fang Chuan Ho, "Influences of the deposition rate on the microstructure and hardness of composite films by reactive ion-assisted coevaporation", Opt. Eng. **34**, 3075-3082 (1995)
9. S.M. Edlou, A. Smajkiewicz and G.A. Al-Jumaily, "Optical properties and environmental stability of oxide coatings deposited by reactive sputtering", Appl. Opt. **32**, 5601-5605 (1993)
10. A. Zöller, R. Götzelmann, K. Matl and D. Cushing, "Temperature-stable bandpass filters deposited with plasma ion-assisted deposition", Appl. Opt. **35**, 5609-5612 (1996)
11. M. Cevro and G. Carter, "Ion-beam and dual-ion-beam sputter deposition of tantalum oxide films", Opt. Eng. 34, 596-606 (1995)
12. N.K. Sahoo and A.P. Shapiro, "Process-parameter-dependent optical and structural properties of ZrO_2MgO mixed-composite films evaporated from the solid solution", Appl. Opt., **37**, 698-718 (1998)

13. E.N. Farabaugh and D.M. Sanders, "Microstructure of dielectric thin films formed by e-beam coevaporation," J. Vac. Sci. Technol. A **1**, 356-359 (1983)
14. S.B. Qadri, E.F. Skelton, P.Lubitz, N.V. Nguyen and H.R. Khan, "Electron beam deposition of ZrO_2-ZnO films," Thin Solid Films **290-291**, 80-83 (1996)
15. Wen-Chou Tsai and Tseung-Yuen Tseng, "Chracterization of yttria-stabilized zirconia thin films grown by planar magnetron sputtering", Thin Solid Films **306**, 86-91 (1997)
16. Fletcher Jones, "High-rate reactive sputter deposition of zirconium dioxide," J. Vac. Sci. Technol. A **6**, 3088-3097 (1988)
17. D. Reicher and K. Jungling, "Influence of crystal structure on the light scatter of zirconium oxide films", Appl. Opt. **36**, 1626-1637 (1997)
18. R.H.J. Hannink, "Growth morphology of the tetragonal phase in partially stabilized zirconia, J. Mater. Sci. 13, 2487-2496 (1978)
19. D. L. Porter and A. H. Heuer, "Microstructural development in MgO-stabilized zirconia (Mg-PSZ)," J. Am. Ceram. Soc. **62**, 298-305 (1979)
20. C.M. Gilmore, C. Quinn, S.B. Qadri, C.R. Gosset and E.F. Skelton, "Stabilization of tetragonal ZrO_2 with Al_2O_3 in reactive magnetron sputtered thin films," J. Vac. Sci. Technol. A **5**, 2085-2087 (1987)
21. O. Ruff and F. Ebert, "Ceramics of highly refractory materials," Z. Anorg. Allgem. Chem. **180**, 19-41 (1929)
22. P. Duwez and F. Odell, "Phase relationships in the system Zirconia-Ceria," J. Am. Ceram. Soc. **33**, 274-283 (1950)
23. N.K. Sahoo and K.V.S.R. Apparao, "Process-parameter optimization of Sb_2O_3 films in the ultraviolet and visible region for interferometric applications," Appl. Phys. A **63**, 195-202 (1996)
24. D. Minkov and R. Swanepoel, "Computer drawing of the envelopes of spectra with interference", K.H. Guenther ed., Proc. SPIE **1782**, 212-220 (1992)
25. A.V. Tikhonravov, M.K. Trubetskov, B.T. Sullivan and J.A. Dobrowolski, "Influence of small inhomogeneities on the spectral characteristics of single thin films", Appl. Opt., **36**, 7188-7198 (1997)
26. J.P. Borgogno, B. Lazarides and E. Pelletier, "Automatic determination of the optical constants of inhomogeneous thin films," Appl. Opt. **21**, 4020-4029 (1982)

27. B. Bovard, F.J. Van Milligen, M.J. Messerly, S.G. Saxe and H.A. Macleod, "Optical constants derivation for an inhomogeneous thin film from in situ transmission measurements," Appl. Opt. **24**, 1803-1807 (1985)

28. E. E. Khawaja, F. Bouamrane, A. B. Hallak, M.A. Daous and M.A. Salim, "Observation of oxygen enrichment in zirconium oxide films," J. Vac. Sci Technol. A **11**, 580-587 (1993)

29. Angela Duparré and Stefan Jakobs, "Combination of surface characterization techniques for investigating optical thin-film components," Appl. Opt. **35**, 5052-5058 (1996)

30. F.Biscarini, P. Samorí, A. Lauria, P. Ostoja, R. Zamboni, C. Taliani, P. Viville, R. Lazzaroni and J.L. Brédas, "Morphology and roughness of high-vacuum sublimed oligomer thin films," Thin Solid Films **284-285**, 439-443 (1996)

31. H.K. Pulker, Coatings on Glass, 2nd ed. (ELSEVIER, New York, 1984), Chap. 8, p.351

32. R.S. Sennett and G.D. Scott, "The structure of evaporated metal films and their optical properties", J.O.S.A. **40**, 203-211 (1950)

Table - 1

Sub. Temp in °C	Coefficient 'A_1'	Coefficient 'A_2'	Coefficient 'A_3' x 10^{-4}	Coefficient 'A_4' x 10^{6}
Ambient	1.6639	9.1580	1.87400	1.5543
125	1.8311	8.8842×10^{-7}	3.68780	2.1931
150	1.8017	0.6229	0.60306	2.4575
162	1.7620	12.9887	0.99827	2.0248
175	1.7665	1.8587	0.44437	2.5131
188	1.8198	3.18×10^{-7}	2.86700	2.8272
200	1.8451	5.312×10^{-7}	2.4668	2.4521
237	1.8539	1.65×10^{-6}	5.7580	1.9179

Table - 2

Sub. Temp in °C	Coefficient 'a'	Coefficient 'b'	Coefficient 'c'	Coefficient 'd'
Ambient	8.1092	3.6645	17.3481	0.8219
125	3.4537	3.3418	15.6766	0.7524
150	1.3125×10^{5}	8.8949	86.7913	1.9691
162	2368.7891	6.6936	61.8524	1.4898
175	4827.6977	7.4023	75.2108	1.6514
188	8.0857×10^{4}	8.9568	92.0650	2.0001
200	372.6082	6.0526	59.3817	1.3480
237	4.6715	3.7362	31.7223	0.8296

Caption to Tables

Table 1: Cauchy coefficients for the films deposited under the same rate of deposition (0.4 nm/s) and with no additional oxygen, but with varying substrate temperatures.

Table 2: Logistic coefficients for the films deposited under the same rate of deposition (0.4 nm/s) and with no additional oxygen, but with varying substrate temperatures.

Caption to Figures

Fig. 1: Transmittance and Reflectance characteristics of the experimental films deposited under substrate temperature of 200 °C, rate 0.4 nm/s and base value of oxygen pressure. Interference peaks in the lower end of the spectra have been considerably modulated because of structural non-linear inhomogeneity.

Fig. 2: Transmittance and Reflectance characteristics of the experimental films deposited under substrate temperature of 162 °C, rate 0.4 nm/s and oxygen pressure of $5x10^{-5}$ mbar. Interference peaks in the lower end of the spectra have also been considerably modulated because of structural non-linear inhomogeneity at this process condition.

Fig. 3: Transmittance and Reflectance characteristics of the experimental films deposited under two extreme experimental substrate temperatures (ambient and 237 °C), rate 0.4 nm/s and base pressure of oxygen. Dispersive behavior in interference peaks clearly indicates the absence of non-linear inhomogeneity. On-line optical monitoring has indicated a fairly homogeneous growth at these conditions.

Fig. 4: Experimental characteristics of an as deposited film measured in air as well as vacuum. Spectral characteristics have shown almost negligible transition between both the measurements.

Fig. 5: Spectral variation of mean refractive index with respect to the substrate temperature. The rates and oxygen pressures were maintained at 0.4 nm/s and base value respectively.

Fig. 6: Spectral variation of mean extinction coefficient with respect to the substrate temperature. The rates and oxygen pressures were maintained at 0.4 nm/s and base value respectively

Fig. 7: Spectral variation of mean refractive index with respect to the rate of deposition. The substrates' temperatures and oxygen pressures were maintained at 162 °C and $1x10^{-4}$ mbar respectively.

Fig. 8: Spectral variation of mean extinction coefficient with respect to the rate of deposition. The substrates' temperatures and oxygen pressures were maintained at 162 °C and $1x10^{-4}$ mbar respectively.

Fig. 9: Spectral variation of mean refractive index with respect to the oxygen pressure. The rates and substrate temperatures were maintained at 0.4 nm/s and 162 °C respectively.

Fig. 10: Spectral variation of mean extinction coefficient with respect to the oxygen pressure. The rates and substrate temperatures were maintained at 0.4 nm/s and 162 °C respectively.

Fig. 11: Surface topography of a composite film deposited under optimum rate of deposition.

Fig. 12: Power Spectral Densities (PSDs) and surface roughness of the films deposited under various substrate temperatures.

Fig. 13: Power Spectral Densities (PSDs) and surface roughness of the films deposited under various rates of deposition.

Fig. 14: Power Spectral Densities (PSDs) and surface roughness of the films deposited under various oxygen pressures.

Fig. 15: Bearing Ratio plots for the films deposited under various substrate temperatures.

Fig. 16: Bearing Ratio plots for the films deposited under various rates of deposition.

Fig. 17: Bearing Ratio plots for the films deposited under various oxygen pressures.

Fig. 18: X-ray diffraction peaks of the films deposited under various deposition rates and oxygen pressures. Some of the films have shown an extremely weak tetragonal structure.

Fig. 19: X-ray diffraction analysis of the films deposited under different substrate temperatures.

Fig. 20: A typical EDX analysis spectrum of a film deposited under substrate temperature 188 °C, rate 0.4 nm/s and without any additional oxygen.

Fig. 21: EDX analyses of the films showing oxygen pressure dependent composition and mean refractive index values.

Fig. 22: EDX analyses of the films showing rate dependent composition and mean refractive index values.

Fig. 23: EDX analyses of the films showing substrate temperature dependent composition and mean refractive index values.

Fig. 24: Experimental spectral characteristic of a metal dielectric filter using Ag and the ternary composite.

Fig. 25: Experimental spectral characteristic of a metal dielectric filter using Ag and the ternary composite.

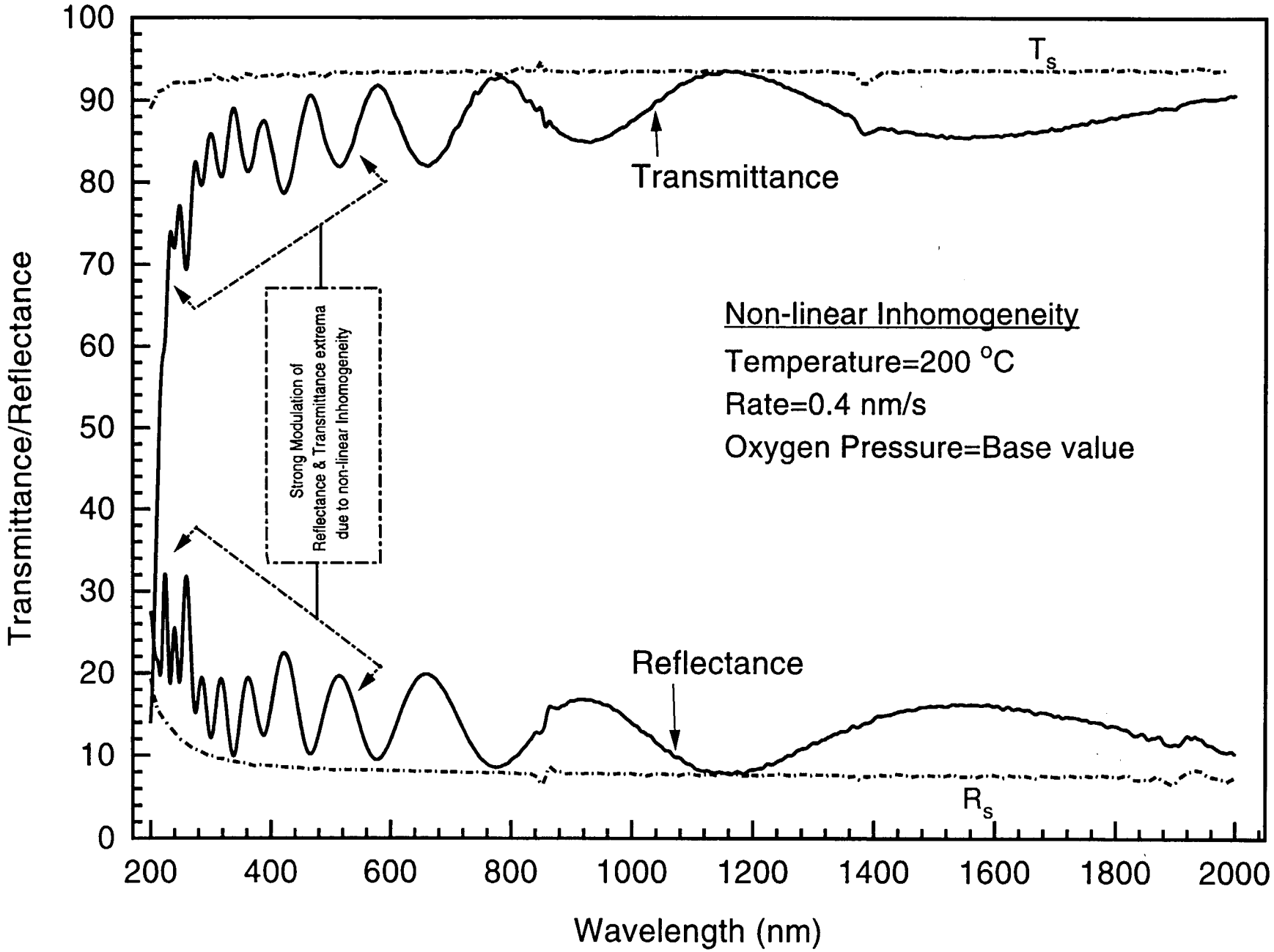
Transmittance/Reflectance
Wavelength (nm)
100
90
80
70
60
50
40
30
20
10
0
200
400
600
800
1000
1200
1400
1600
1800
2000
T_s
Transmittance
Reflectance
R_s
Strong Modulation of Reflectance & Transmittance extrema due to non-linear Inhomogeneity
Non-linear Inhomogeneity
Temperature=200 °C
Rate=0.4 nm/s
Oxygen Pressure=Base value

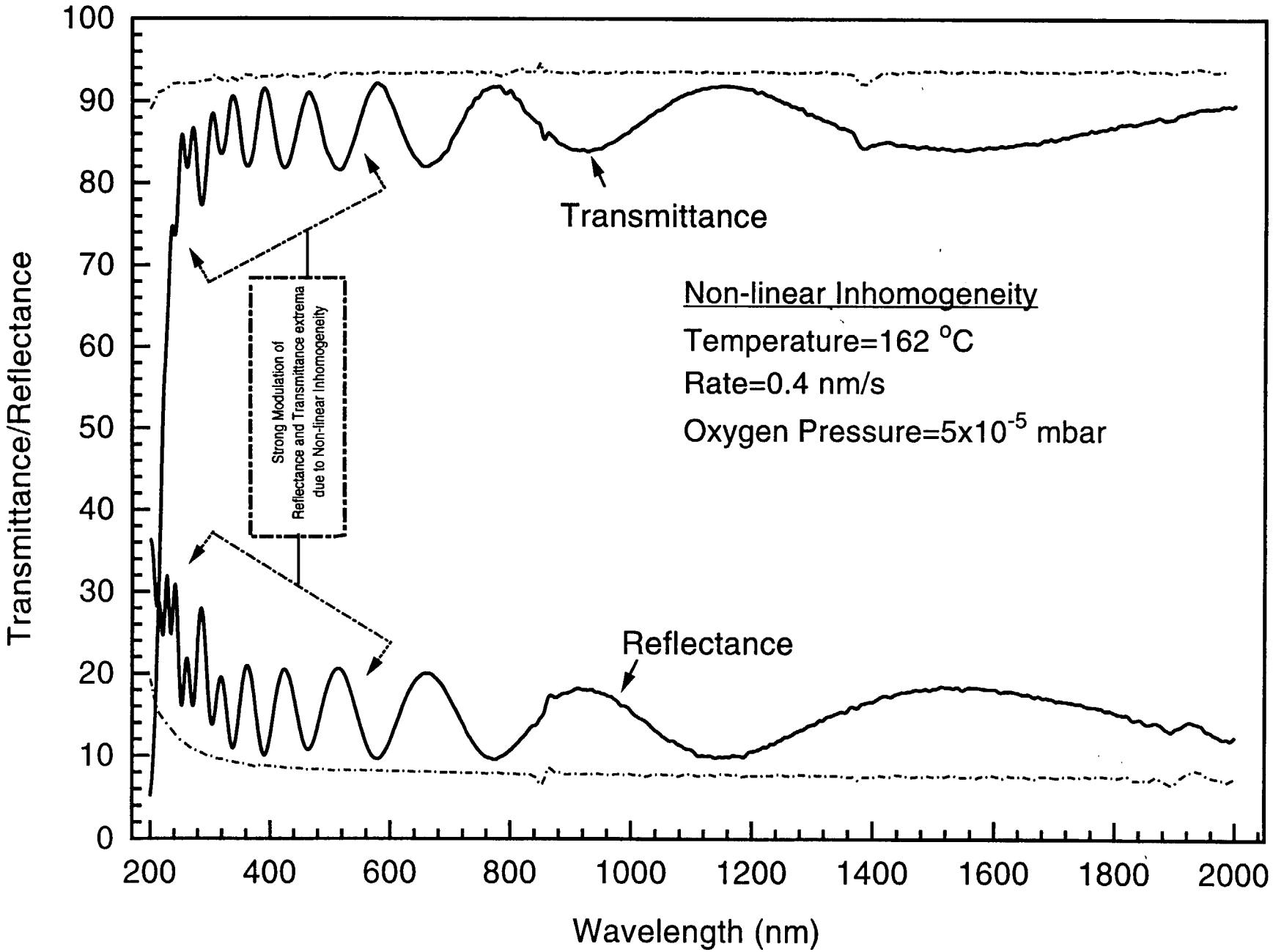
Transmittance/Reflectance
100
90
80
70
60
50
40
30
20
10
0
200
400
600
800
1000
1200
1400
1600
1800
2000
Wavelength (nm)
Transmittance
Reflectance
Strong Modulation of Reflectance and Transmittance extrema due to Non-linear Inhomogeneity
Non-linear Inhomogeneity
Temperature=162 °C
Rate=0.4 nm/s
Oxygen Pressure=5x10-5 mbar

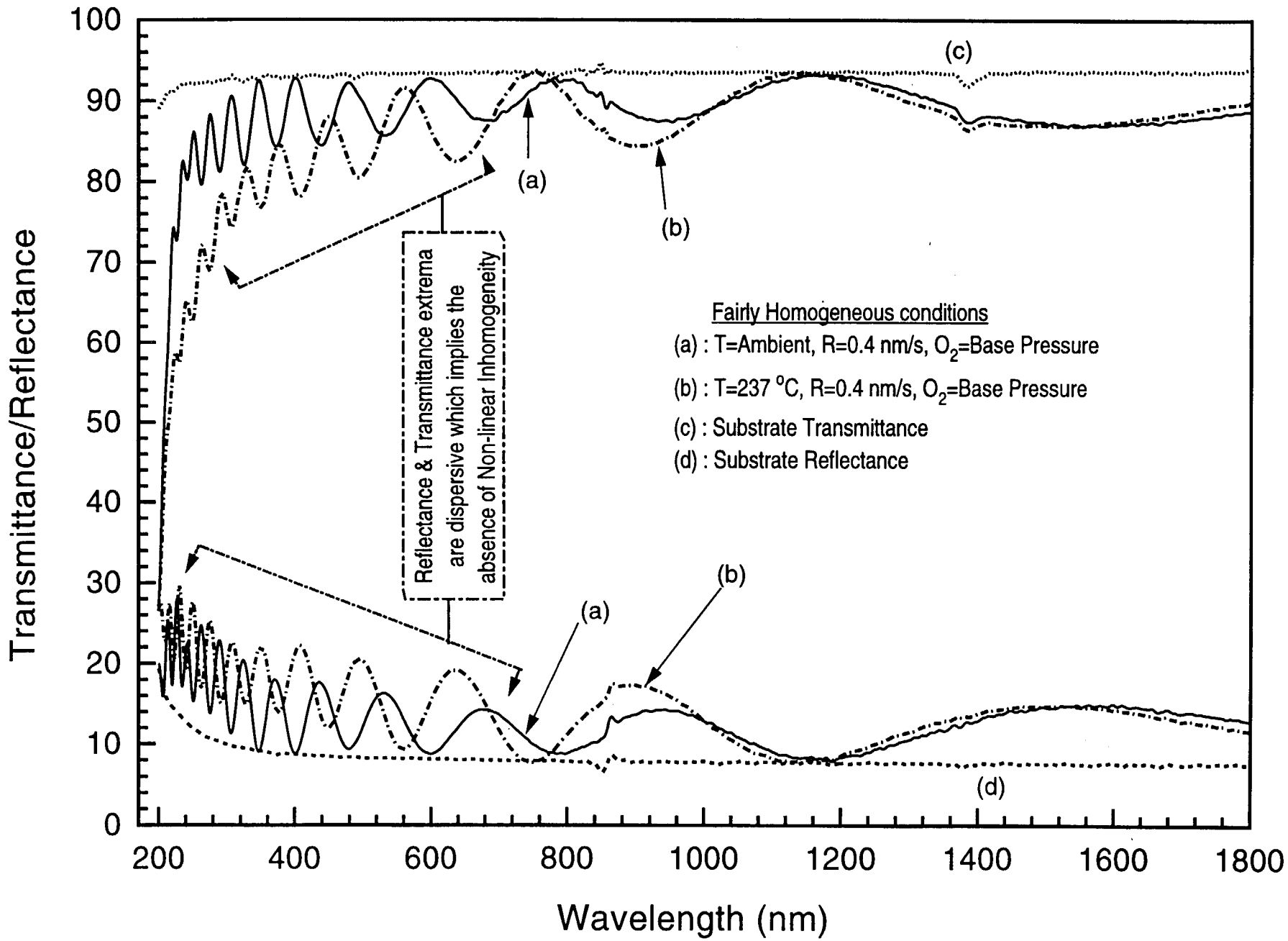
Transmittance/Reflectance
Wavelength (nm)
100
90
80
70
60
50
40
30
20
10
0
200
400
600
800
1000
1200
1400
1600
1800
(a)
(b)
(c)
(d)
Reflectance & Transmittance extrema are dispersive which implies the absence of Non-linear Inhomogeneity
Fairly Homogeneous conditions
(a) : T=Ambient, R=0.4 nm/s, O_2=Base Pressure
(b) : T=237 °C, R=0.4 nm/s, O_2=Base Pressure
(c) : Substrate Transmittance
(d) : Substrate Reflectance

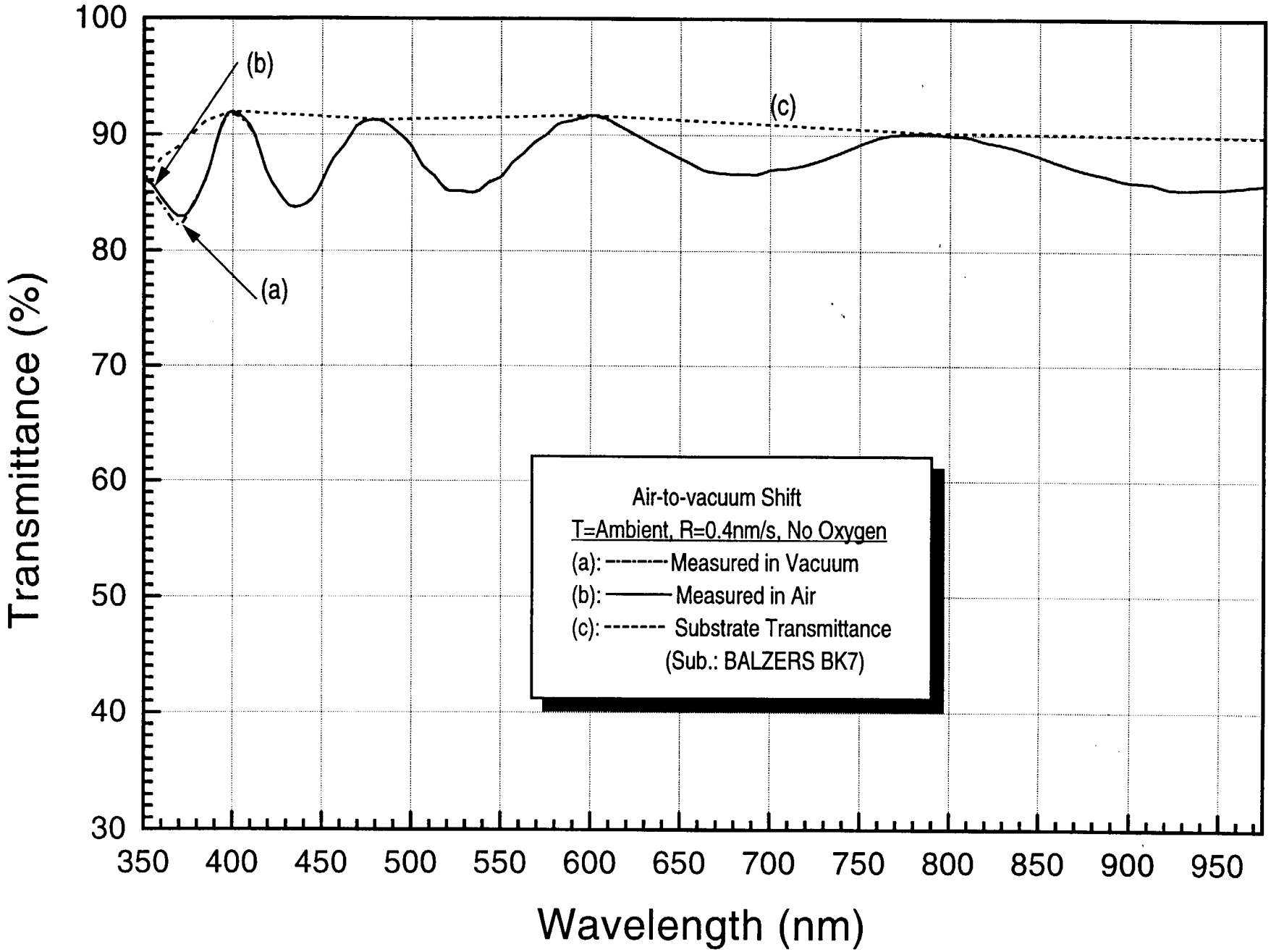
100
90
80
70
60
50
40
30
Transmittance (%)
350
400
450
500
550
600
650
700
750
800
850
900
950
Wavelength (nm)
(a)
(b)
(c)
Air-to-vacuum Shift
T=Ambient, R=0.4nm/s, No Oxygen
(a): Measured in Vacuum
(b): Measured in Air
(c): Substrate Transmittance
(Sub.: BALZERS BK7)

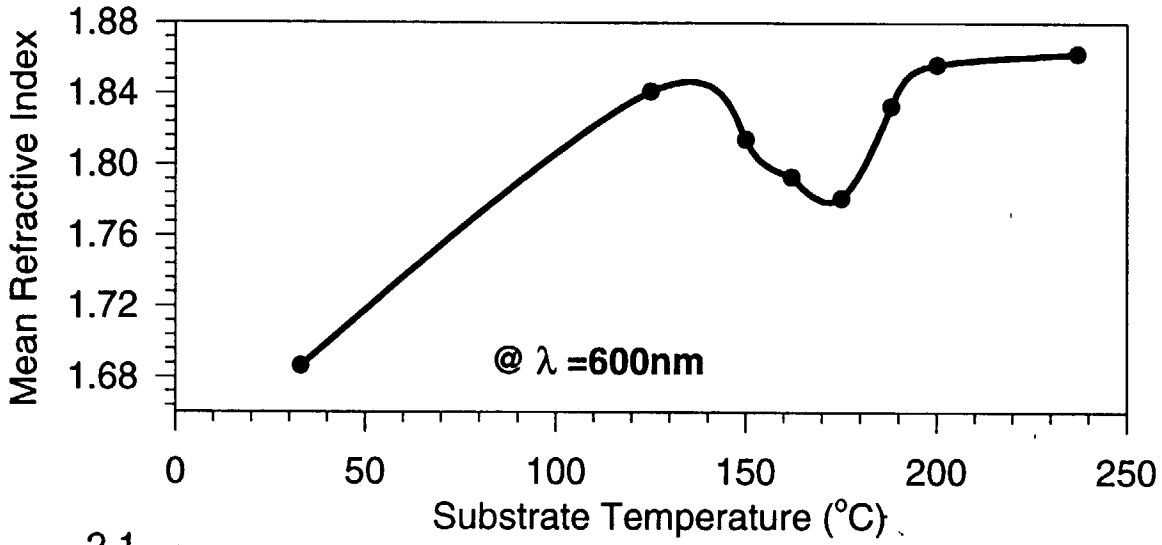
Mean Refractive Index
1.88
1.84
1.80
1.76
1.72
1.68
@ λ =600nm
0
50
100
150
200
250
Substrate Temperature (°C)

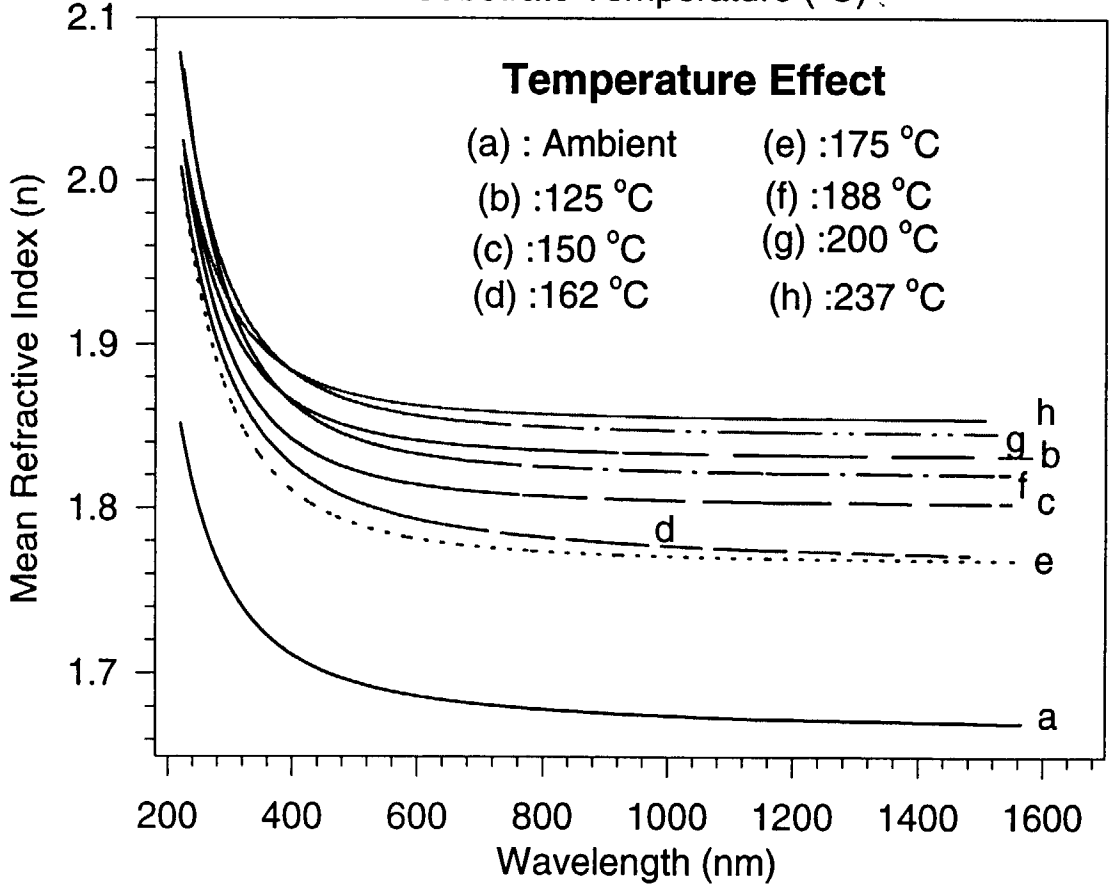
Temperature Effect
(a) : Ambient
(b) :125 °C
(c) :150 °C
(d) :162 °C
(e) :175 °C
(f) :188 °C
(g) :200 °C
(h) :237 °C
Mean Refractive Index (n)
2.1
2.0
1.9
1.8
1.7
h
g
b
f
c
d
e
a
200
400
600
800
1000
1200
1400
1600
Wavelength (nm)

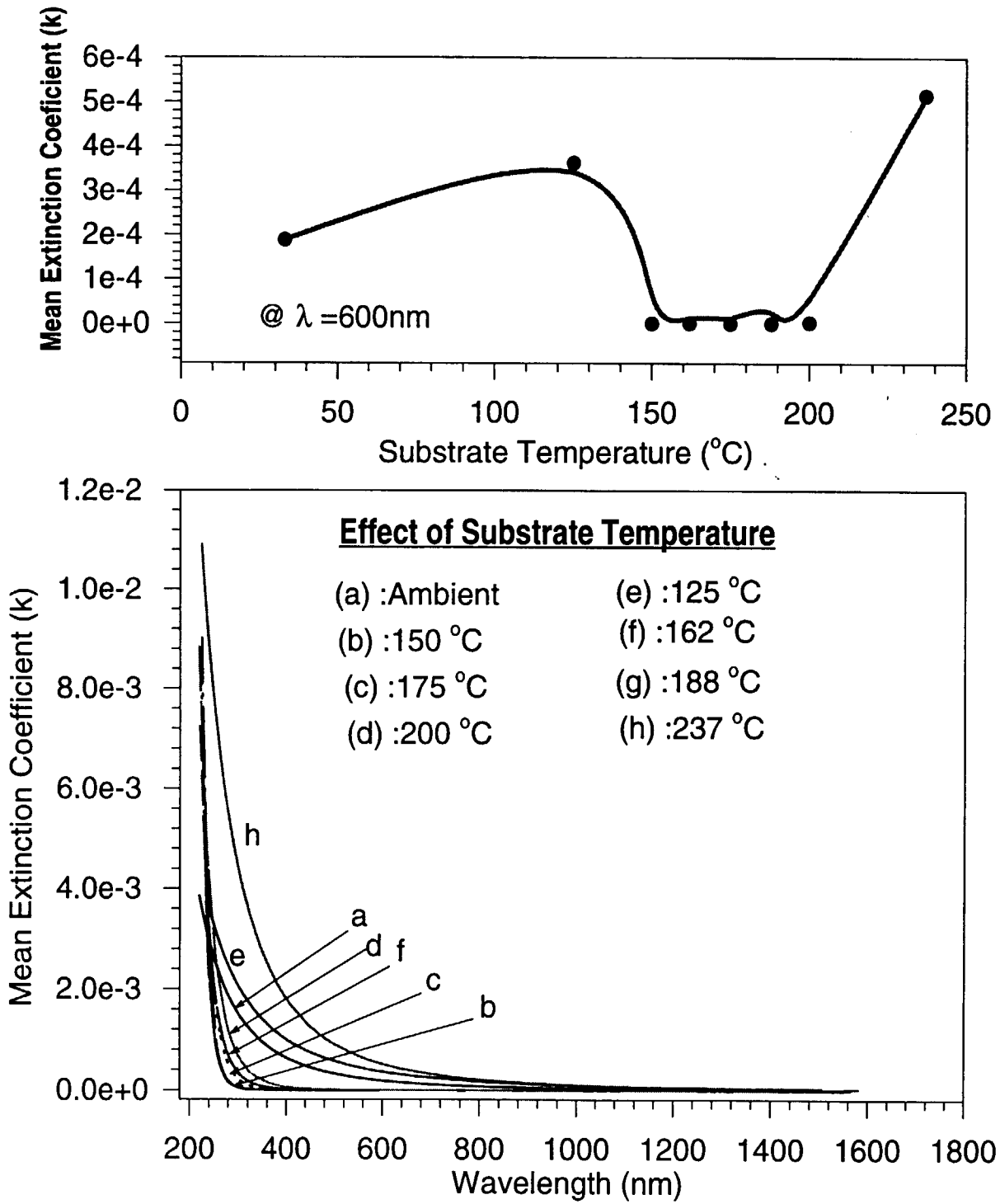
Mean Extinction Coeficient (k)
6e-4
5e-4
4e-4
3e-4
2e-4
1e-4
0e+0
@ λ =600nm
0
50
100
150
200
250
Substrate Temperature (°C)
Effect of Substrate Temperature
(a) :Ambient
(b) :150 °C
(c) :175 °C
(d) :200 °C
(e) :125 °C
(f) :162 °C
(g) :188 °C
(h) :237 °C
Mean Extinction Coefficient (k)
1.2e-2
1.0e-2
8.0e-3
6.0e-3
4.0e-3
2.0e-3
0.0e+0
h
a
d
f
e
c
b
200
400
600
800
1000
1200
1400
1600
1800
Wavelength (nm)

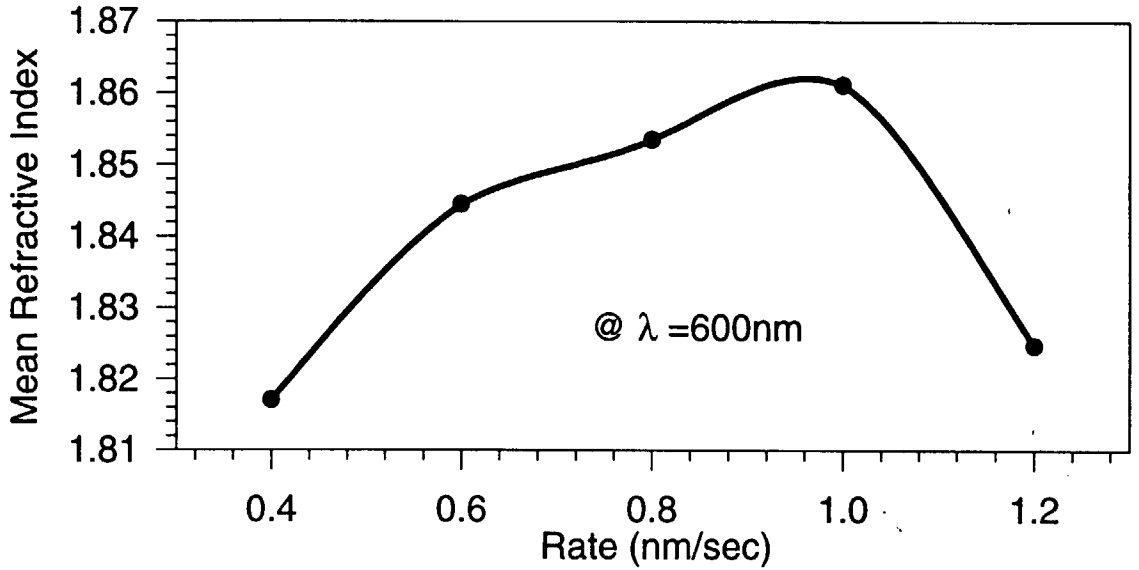
Mean Refractive Index
1.87
1.86
1.85
1.84
1.83
1.82
1.81
@ λ =600nm
0.4
0.6
0.8
1.0
1.2
Rate (nm/sec)

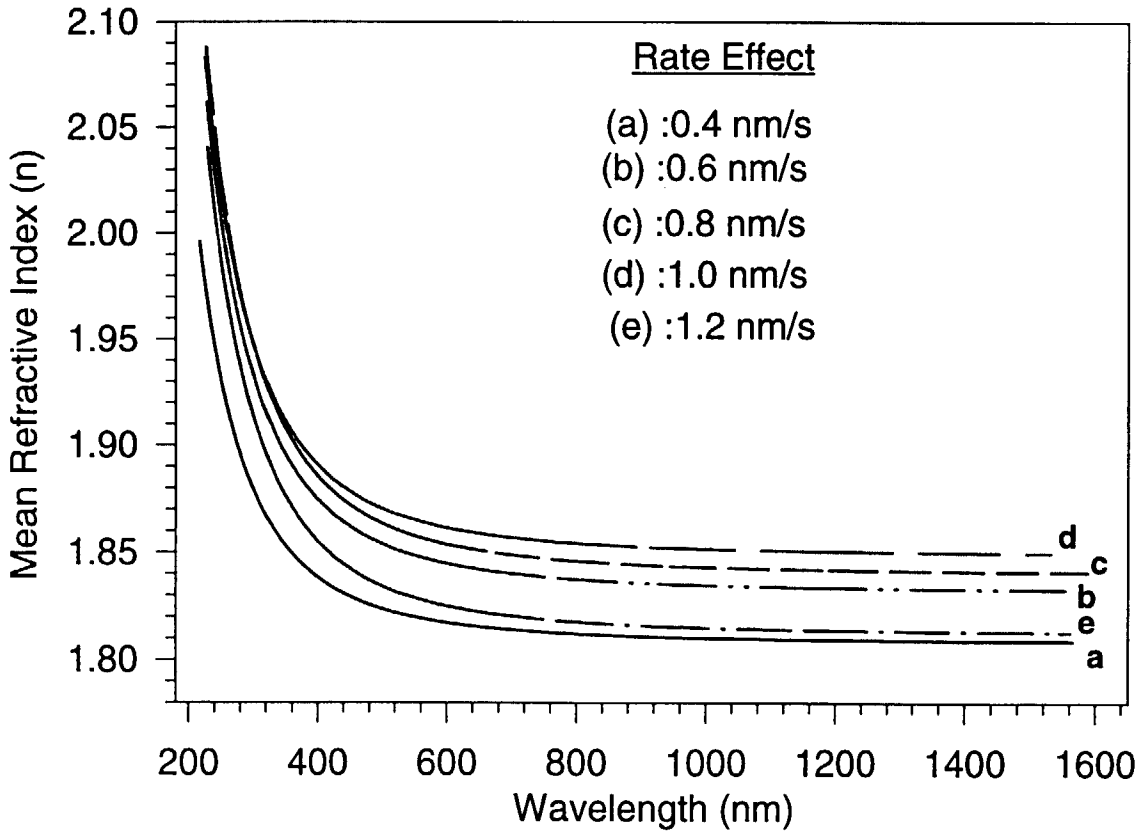
Mean Refractive Index (n)
2.10
2.05
2.00
1.95
1.90
1.85
1.80
Rate Effect
(a) :0.4 nm/s
(b) :0.6 nm/s
(c) :0.8 nm/s
(d) :1.0 nm/s
(e) :1.2 nm/s
d
c
b
e
a
200
400
600
800
1000
1200
1400
1600
Wavelength (nm)

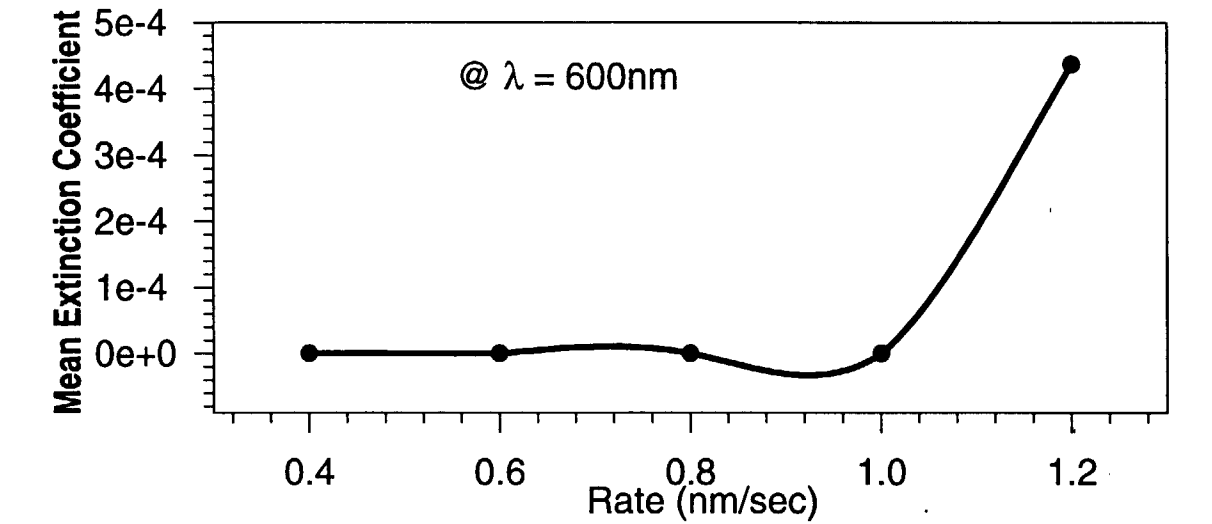
Mean Extinction Coefficient
5e-4
4e-4
3e-4
2e-4
1e-4
0e+0
@ λ = 600nm
0.4
0.6
0.8
1.0
1.2
Rate (nm/sec)

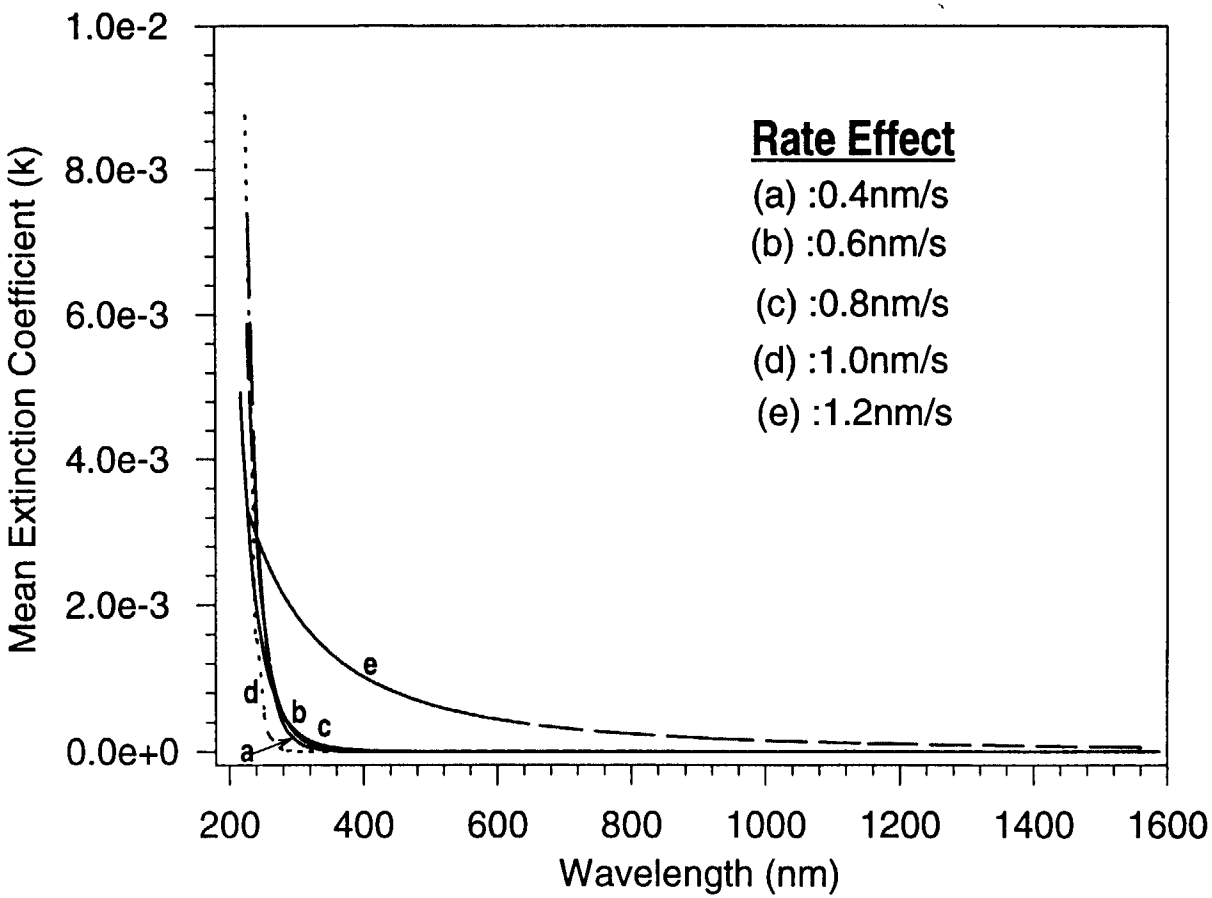
Mean Extinction Coefficient (k)
1.0e-2
8.0e-3
6.0e-3
4.0e-3
2.0e-3
0.0e+0
Rate Effect
(a) :0.4nm/s
(b) :0.6nm/s
(c) :0.8nm/s
(d) :1.0nm/s
(e) :1.2nm/s
a
b
c
d
e
200
400
600
800
1000
1200
1400
1600
Wavelength (nm)

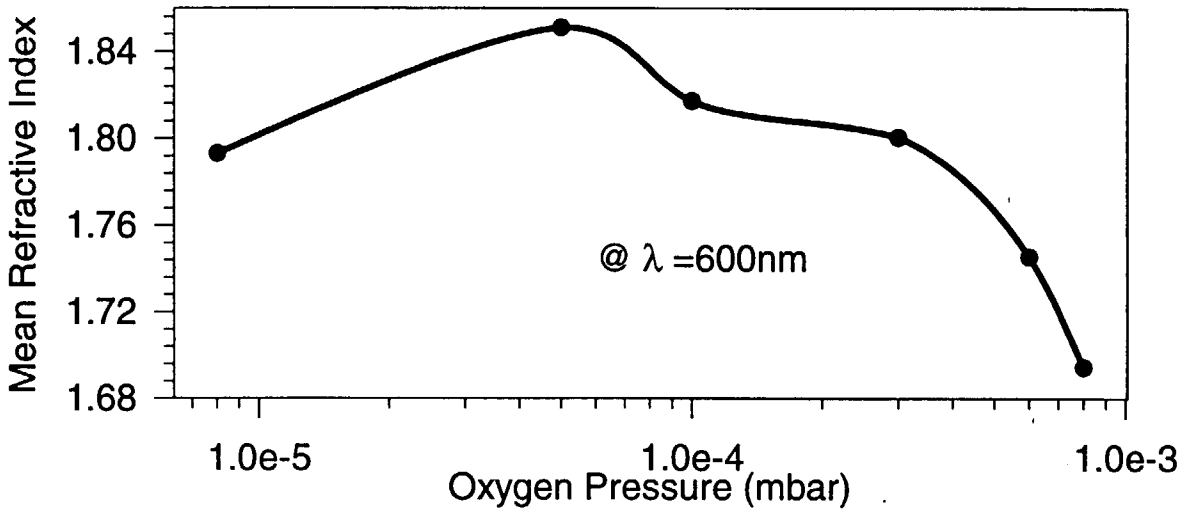
Mean Refractive Index
1.84
1.80
1.76
1.72
1.68
@ λ =600nm
1.0e-5
1.0e-4
1.0e-3
Oxygen Pressure (mbar)

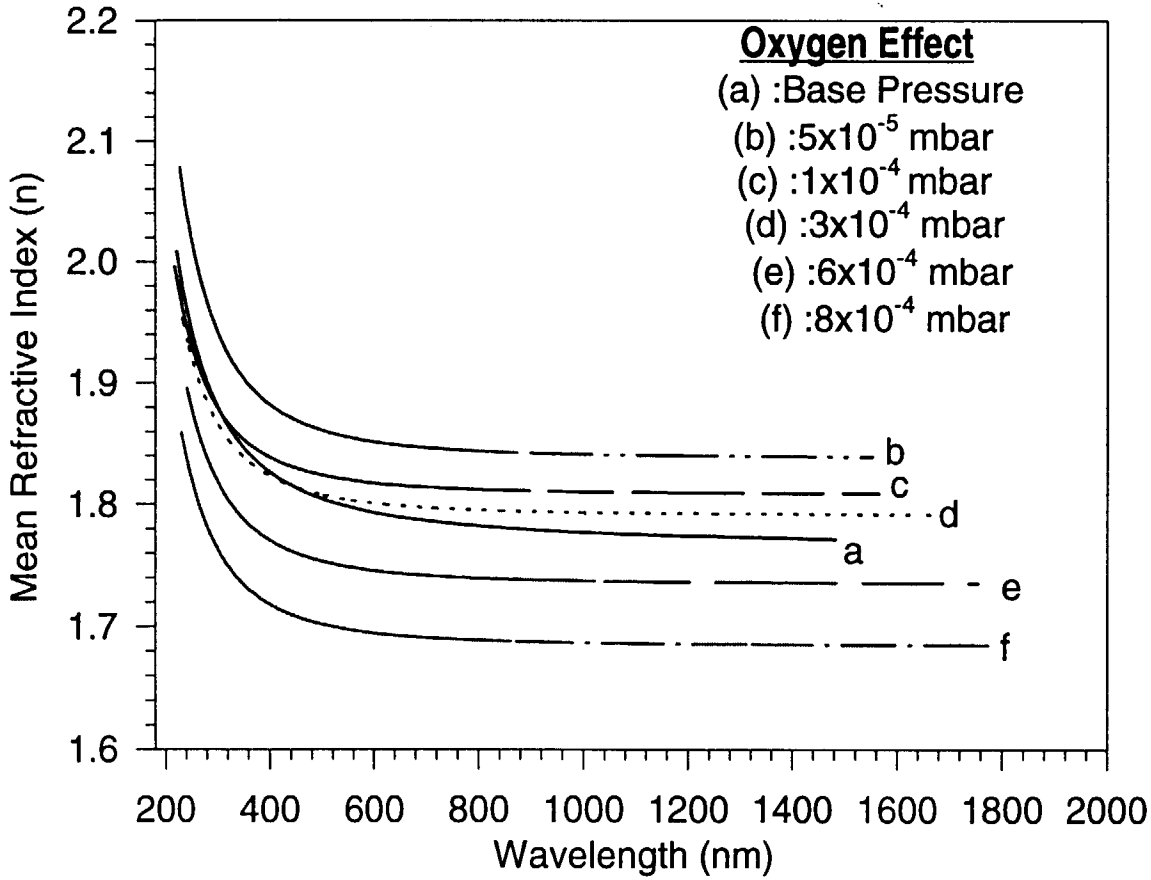
Oxygen Effect
(a) :Base Pressure
(b) :5x10-5 mbar
(c) :1x10-4 mbar
(d) :3x10-4 mbar
(e) :6x10-4 mbar
(f) :8x10-4 mbar
Mean Refractive Index (n)
2.2
2.1
2.0
1.9
1.8
1.7
1.6
a
b
c
d
e
f
200
400
600
800
1000
1200
1400
1600
1800
2000
Wavelength (nm)

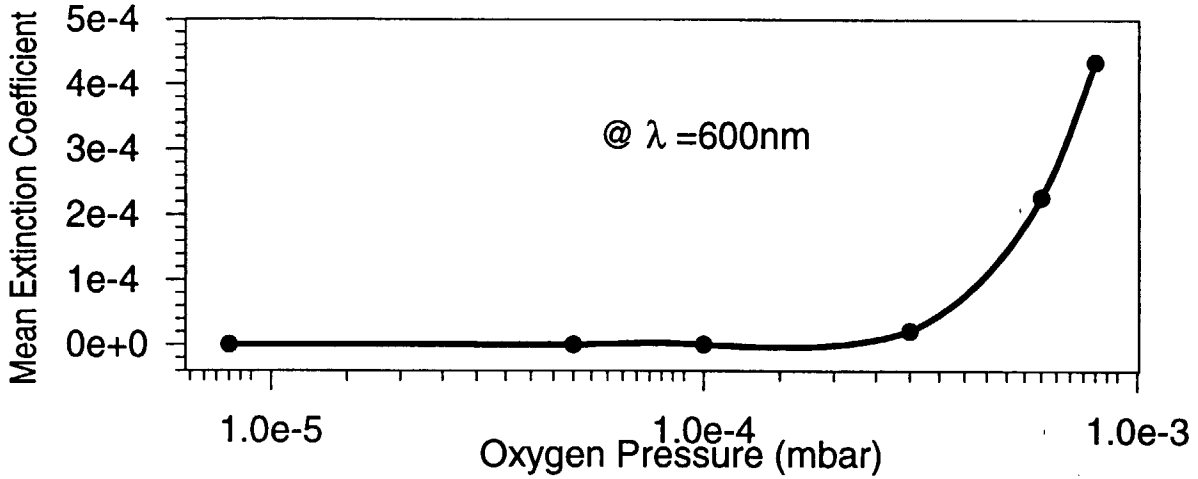
Mean Extinction Coefficient
5e-4
4e-4
3e-4
2e-4
1e-4
0e+0
@ λ =600nm
1.0e-5
1.0e-4
1.0e-3
Oxygen Pressure (mbar)

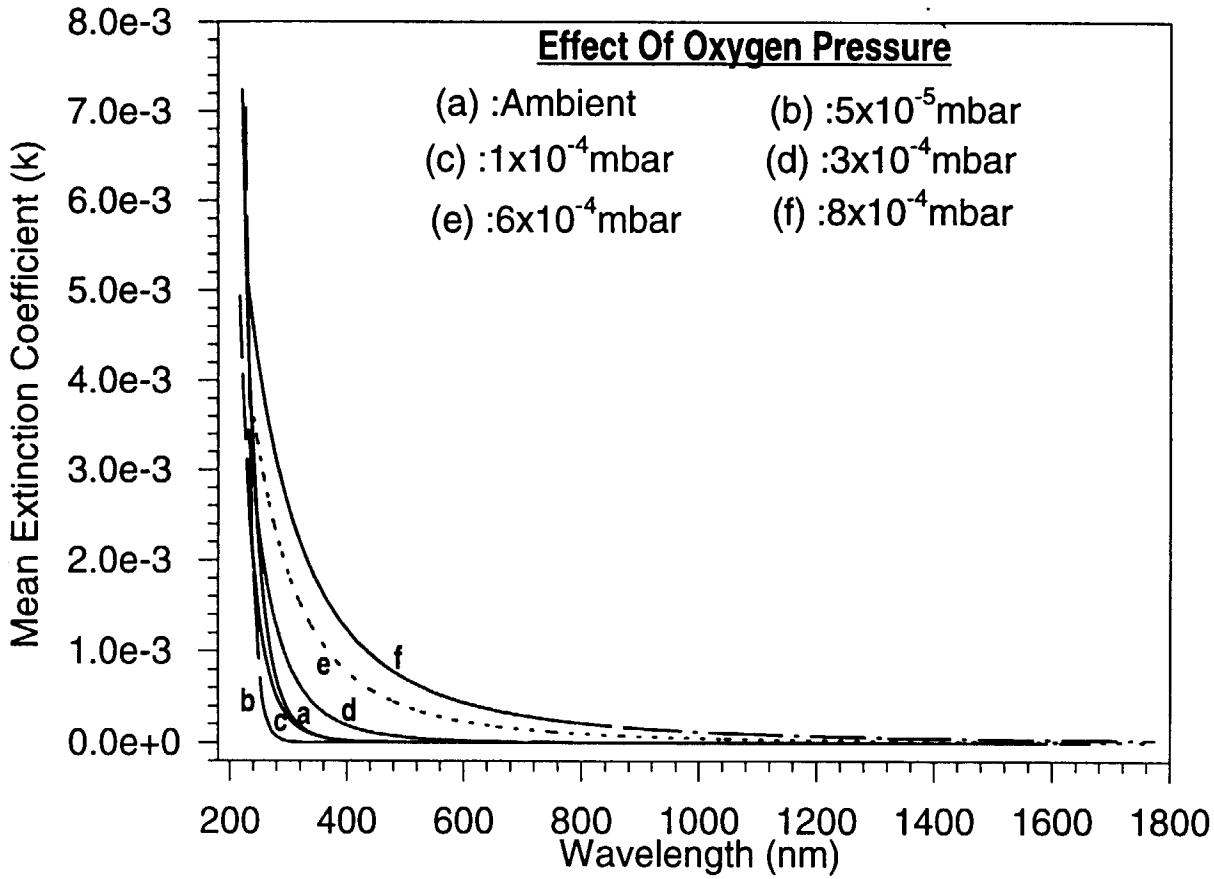
Effect Of Oxygen Pressure
(a) :Ambient
(b) :5x10-5mbar
(c) :1x10-4mbar
(d) :3x10-4mbar
(e) :6x10-4mbar
(f) :8x10-4mbar
Mean Extinction Coefficient (k)
8.0e-3
7.0e-3
6.0e-3
5.0e-3
4.0e-3
3.0e-3
2.0e-3
1.0e-3
0.0e+0
a
b
c
d
e
f
200
400
600
800
1000
1200
1400
1600
1800
Wavelength (nm)

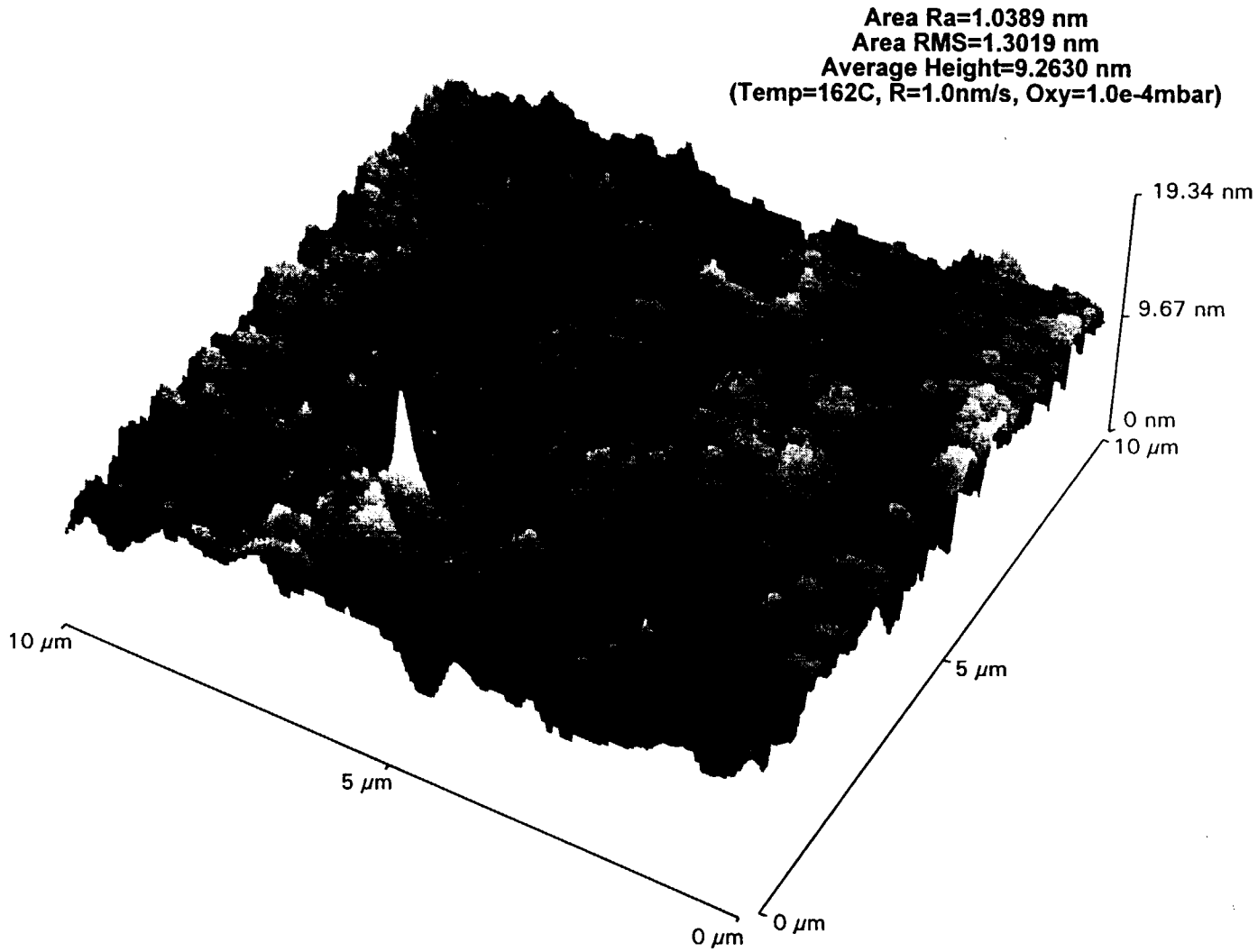
Area Ra=1.0389 nm
Area RMS=1.3019 nm
Average Height=9.2630 nm
(Temp=162C, R=1.0nm/s, Oxy=1.0e-4mbar)
19.34 nm
9.67 nm
0 nm
10 μm
5 μm
0 μm
10 μm
5 μm
0 μm

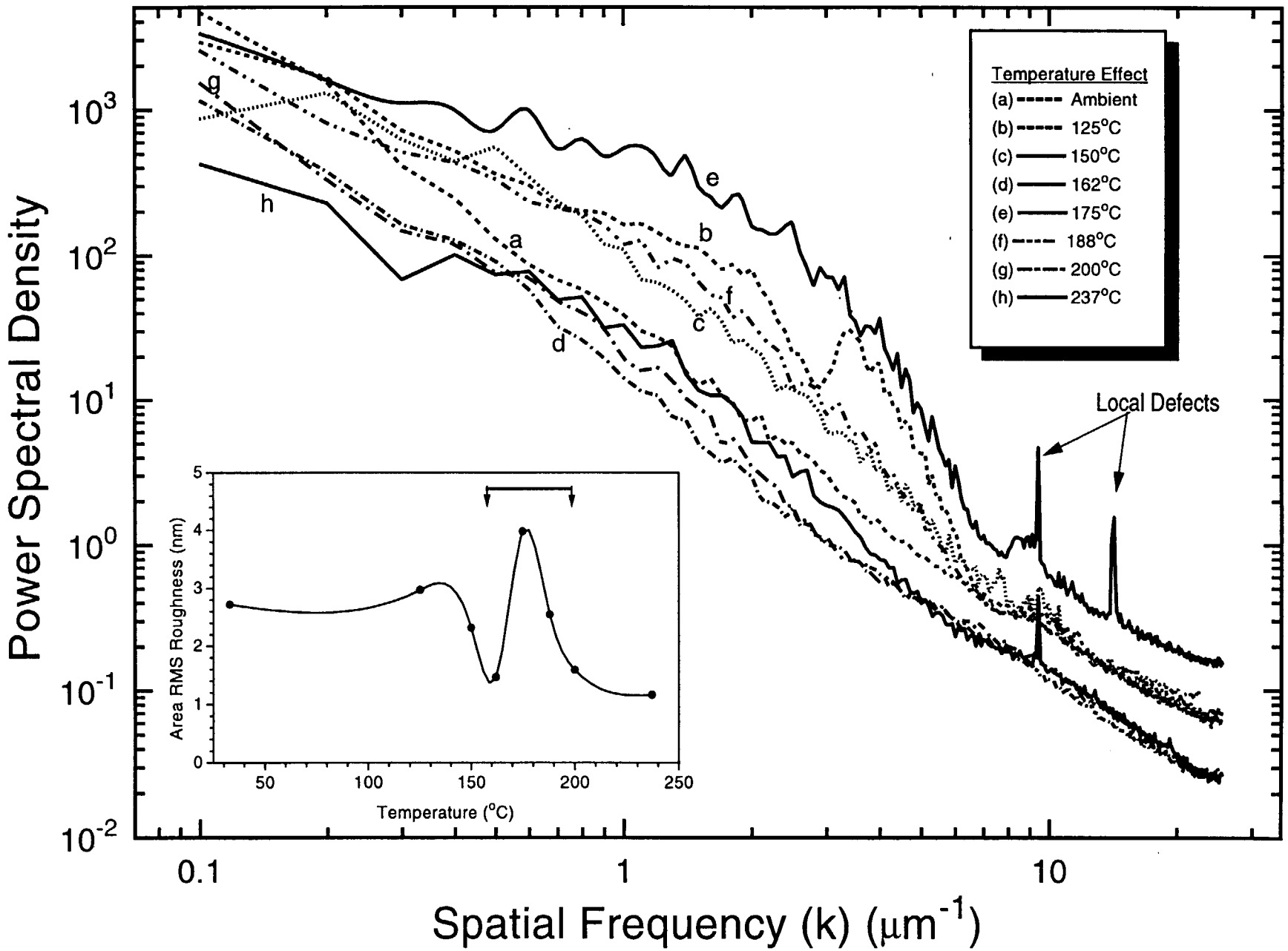
Power Spectral Density
Spatial Frequency (k) (μm-1)
Temperature Effect
(a) Ambient
(b) 125°C
(c) 150°C
(d) 162°C
(e) 175°C
(f) 188°C
(g) 200°C
(h) 237°C
Local Defects
Area RMS Roughness (nm)
Temperature (°C)

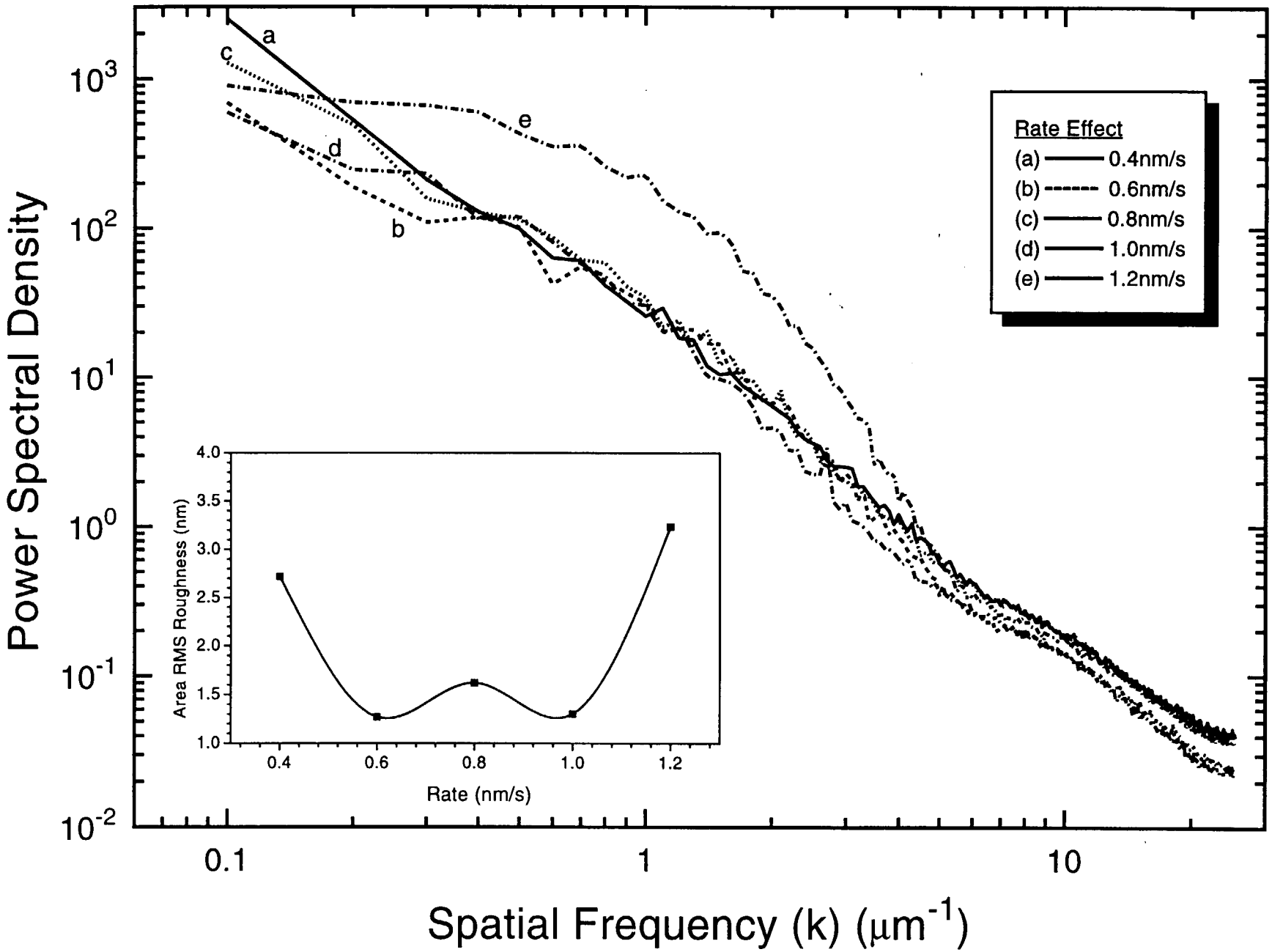
Power Spectral Density
Spatial Frequency (k) (μm-1)
10^3
10^2
10^1
10^0
10^-1
10^-2
0.1
1
10
a
b
c
d
e
Rate Effect
(a) 0.4nm/s
(b) 0.6nm/s
(c) 0.8nm/s
(d) 1.0nm/s
(e) 1.2nm/s
Area RMS Roughness (nm)
4.0
3.5
3.0
2.5
2.0
1.5
1.0
0.4
0.6
0.8
1.0
1.2
Rate (nm/s)

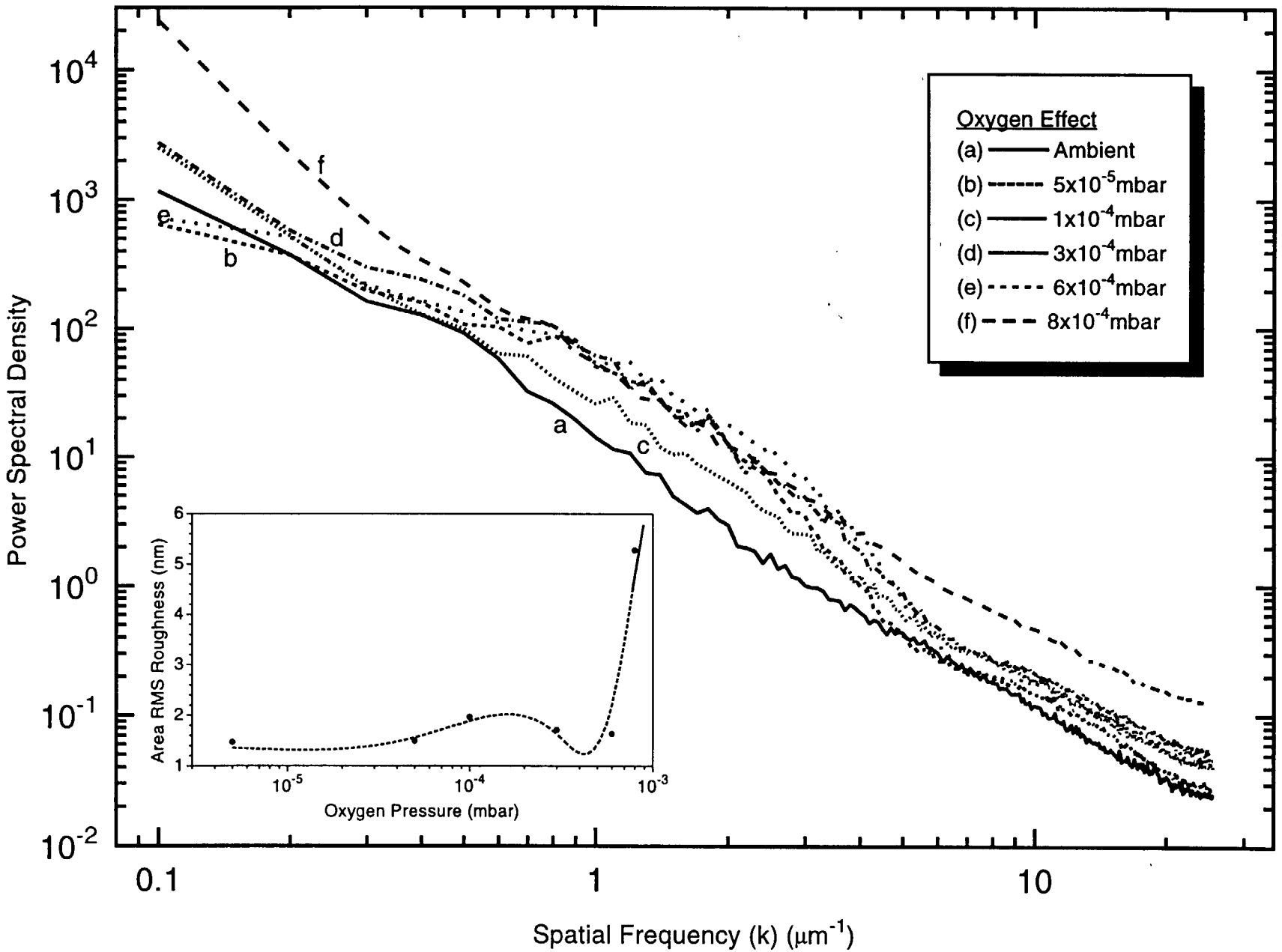
Power Spectral Density
Spatial Frequency (k) (μm-1)
Oxygen Effect
(a) Ambient
(b) 5x10-5mbar
(c) 1x10-4mbar
(d) 3x10-4mbar
(e) 6x10-4mbar
(f) 8x10-4mbar
a
b
c
d
e
f
Area RMS Roughness (nm)
Oxygen Pressure (mbar)

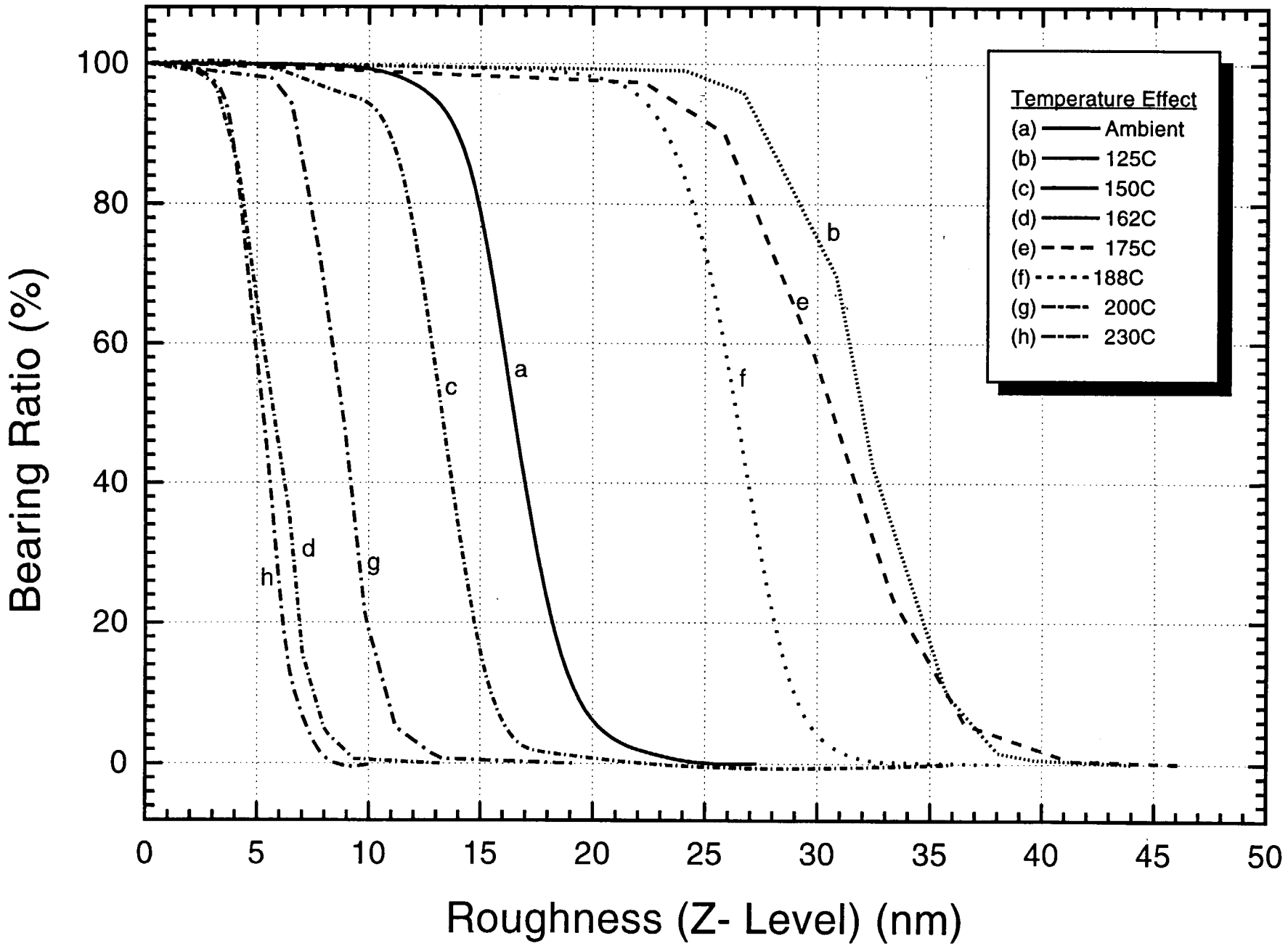
Bearing Ratio (%)
100
80
60
40
20
0
0
5
10
15
20
25
30
35
40
45
50
Roughness (Z- Level) (nm)
Temperature Effect
(a) Ambient
(b) 125C
(c) 150C
(d) 162C
(e) 175C
(f) 188C
(g) 200C
(h) 230C
a
b
c
d
e
f
g
h

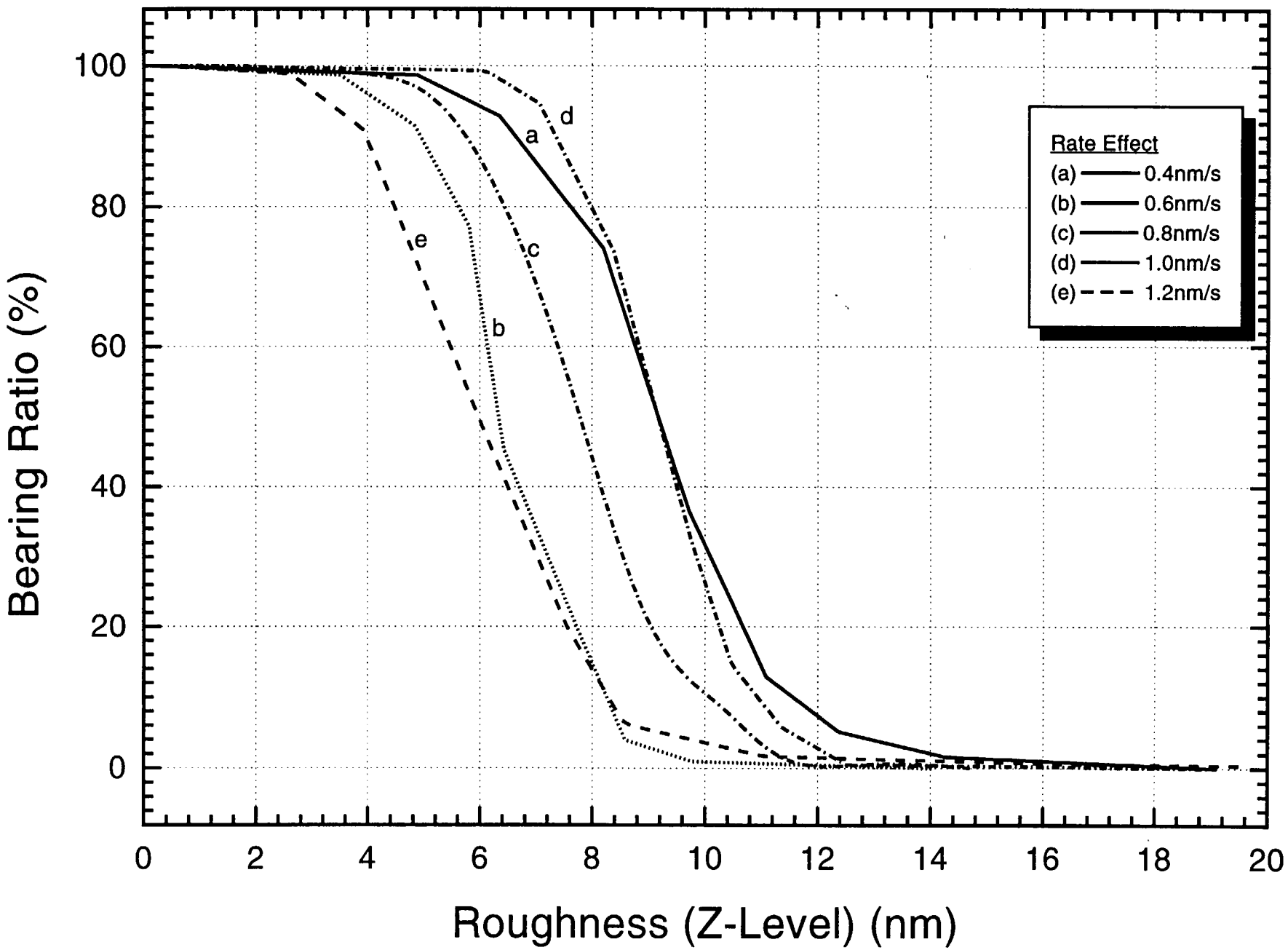
Bearing Ratio (%)
100
80
60
40
20
0
0
2
4
6
8
10
12
14
16
18
20
Roughness (Z-Level) (nm)
a
b
c
d
e
Rate Effect
(a) 0.4nm/s
(b) 0.6nm/s
(c) 0.8nm/s
(d) 1.0nm/s
(e) 1.2nm/s

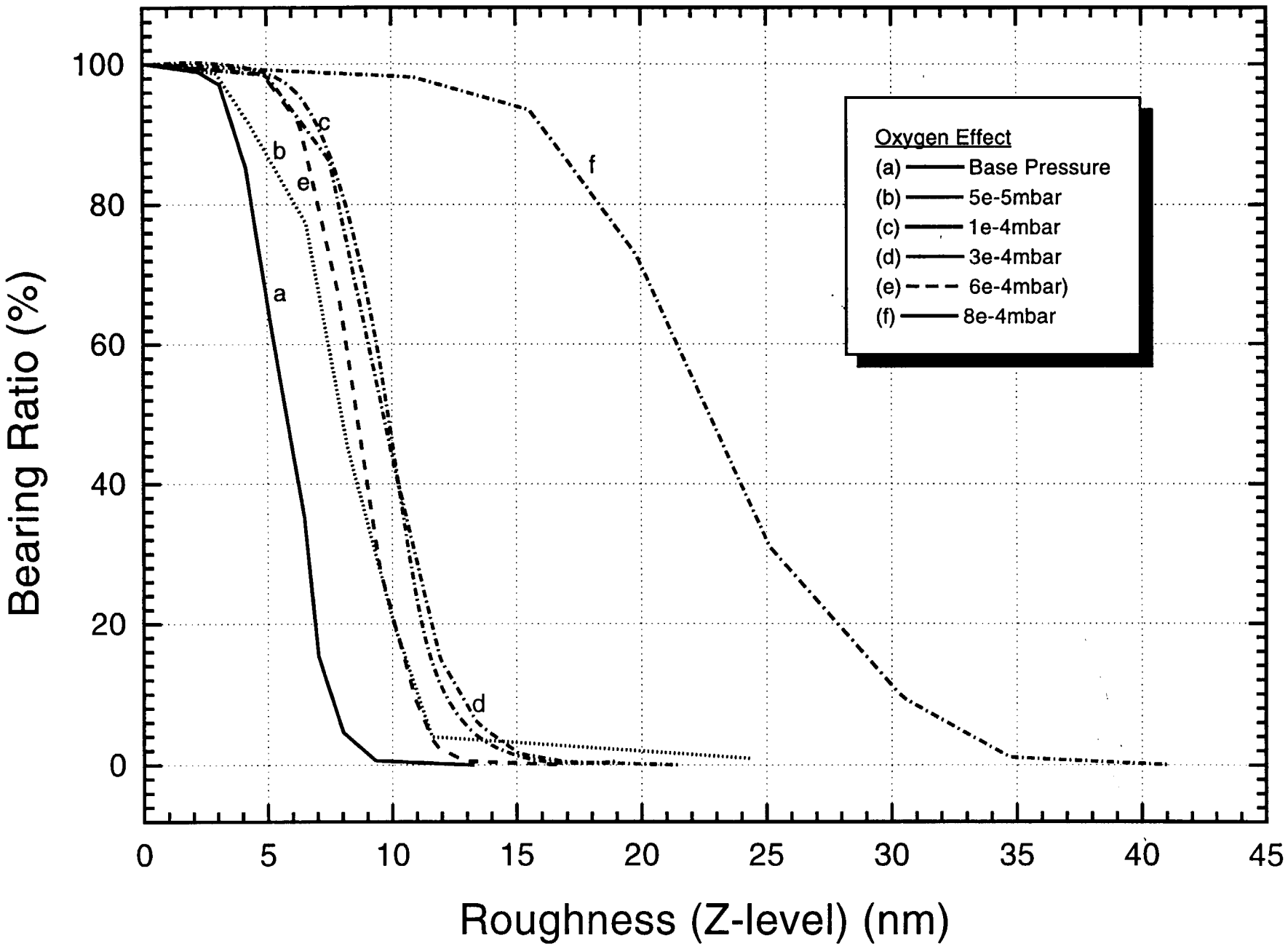
Bearing Ratio (%)
100
80
60
40
20
0
0
5
10
15
20
25
30
35
40
45
Roughness (Z-level) (nm)
Oxygen Effect
(a) Base Pressure
(b) 5e-5mbar
(c) 1e-4mbar
(d) 3e-4mbar
(e) 6e-4mbar)
(f) 8e-4mbar
a
b
c
d
e
f

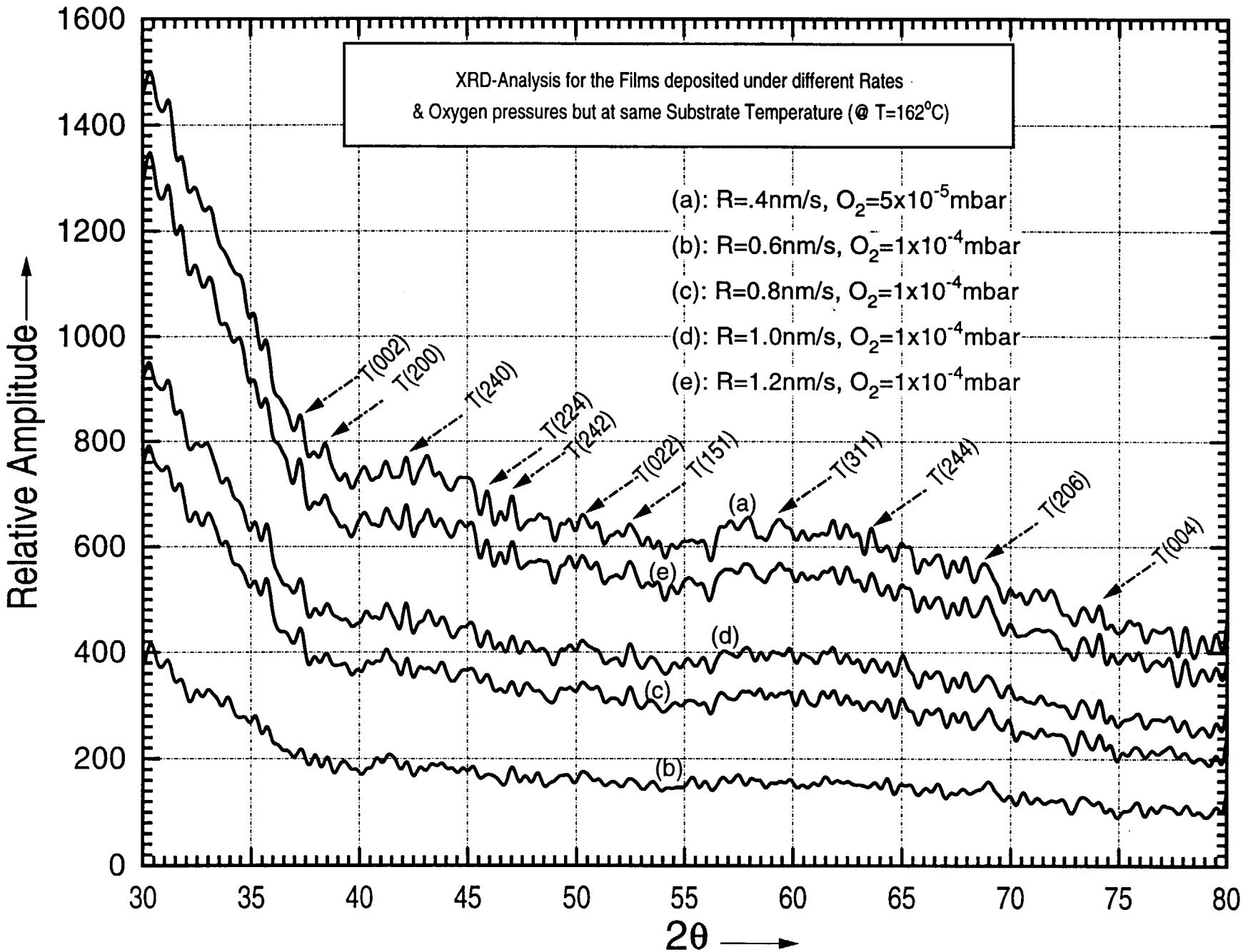
XRD-Analysis for the Films deposited under different Rates
& Oxygen pressures but at same Substrate Temperature (@ T=162°C)
(a): R=.4nm/s, O2=5x10-5mbar
(b): R=0.6nm/s, O2=1x10-4mbar
(c): R=0.8nm/s, O2=1x10-4mbar
(d): R=1.0nm/s, O2=1x10-4mbar
(e): R=1.2nm/s, O2=1x10-4mbar
T(002)
T(200)
T(240)
T(224)
T(242)
T(022)
T(151)
T(311)
T(244)
T(206)
T(004)
(a)
(e)
(d)
(c)
(b)
Relative Amplitude
2θ
0
200
400
600
800
1000
1200
1400
1600
30
35
40
45
50
55
60
65
70
75
80

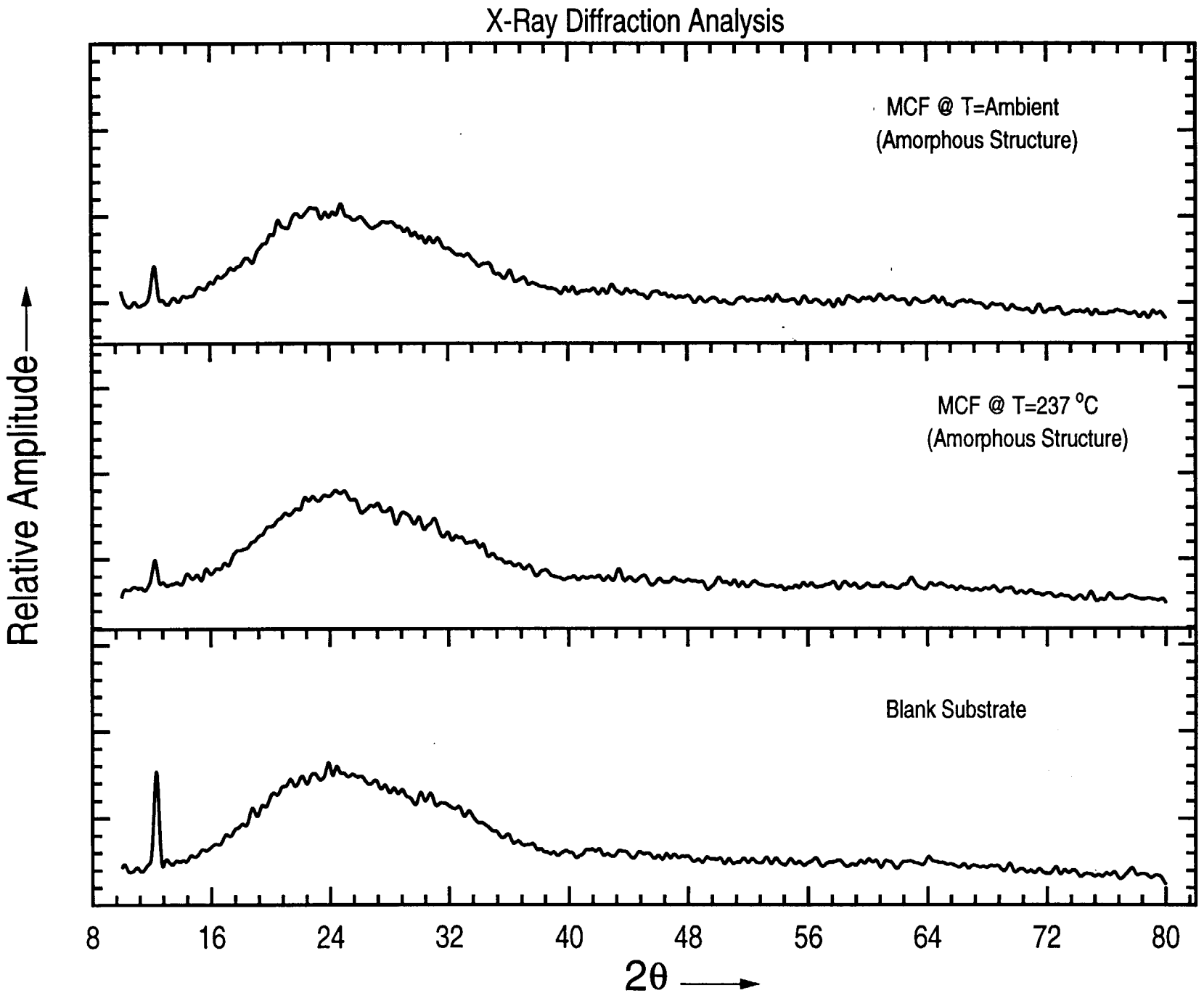
X-Ray Diffraction Analysis
MCF @ T=Ambient
(Amorphous Structure)
MCF @ T=237 °C
(Amorphous Structure)
Blank Substrate
Relative Amplitude
8
16
24
32
40
48
56
64
72
80
2θ

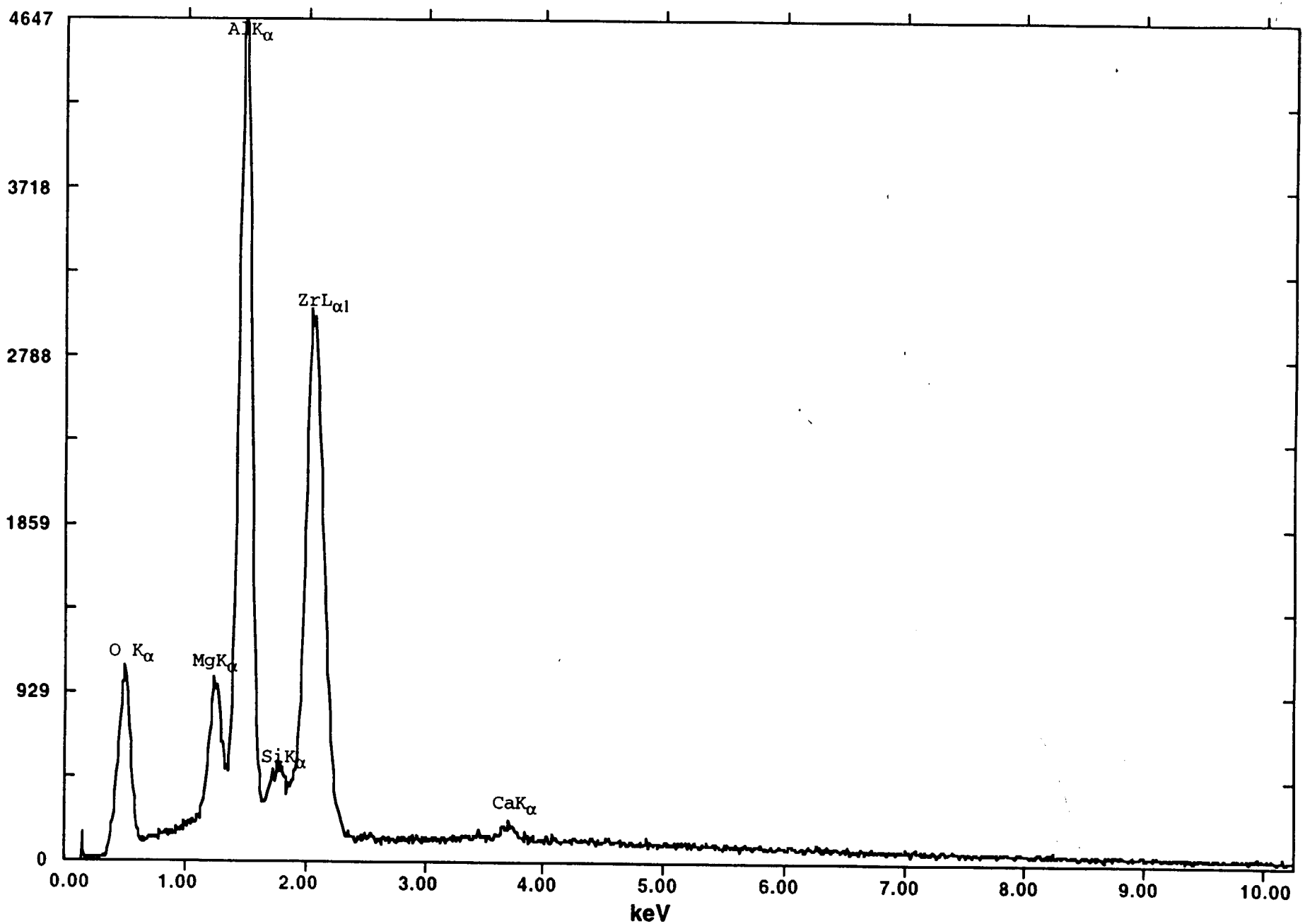

MG/AL/ZR-OXIDE FILM ON BK7 GLASS DISK

SAMPLE #10

Analyst: COSTON/SMITHERS keV: 10.00 Current: 0.50 Live Time: 100.00 eV/Channel= 10.00

Detector Resolution: 145.00 eV Take-off angle= 35.00 Spectrum # 1 From the file: 1997-199 Spectrum.Dat

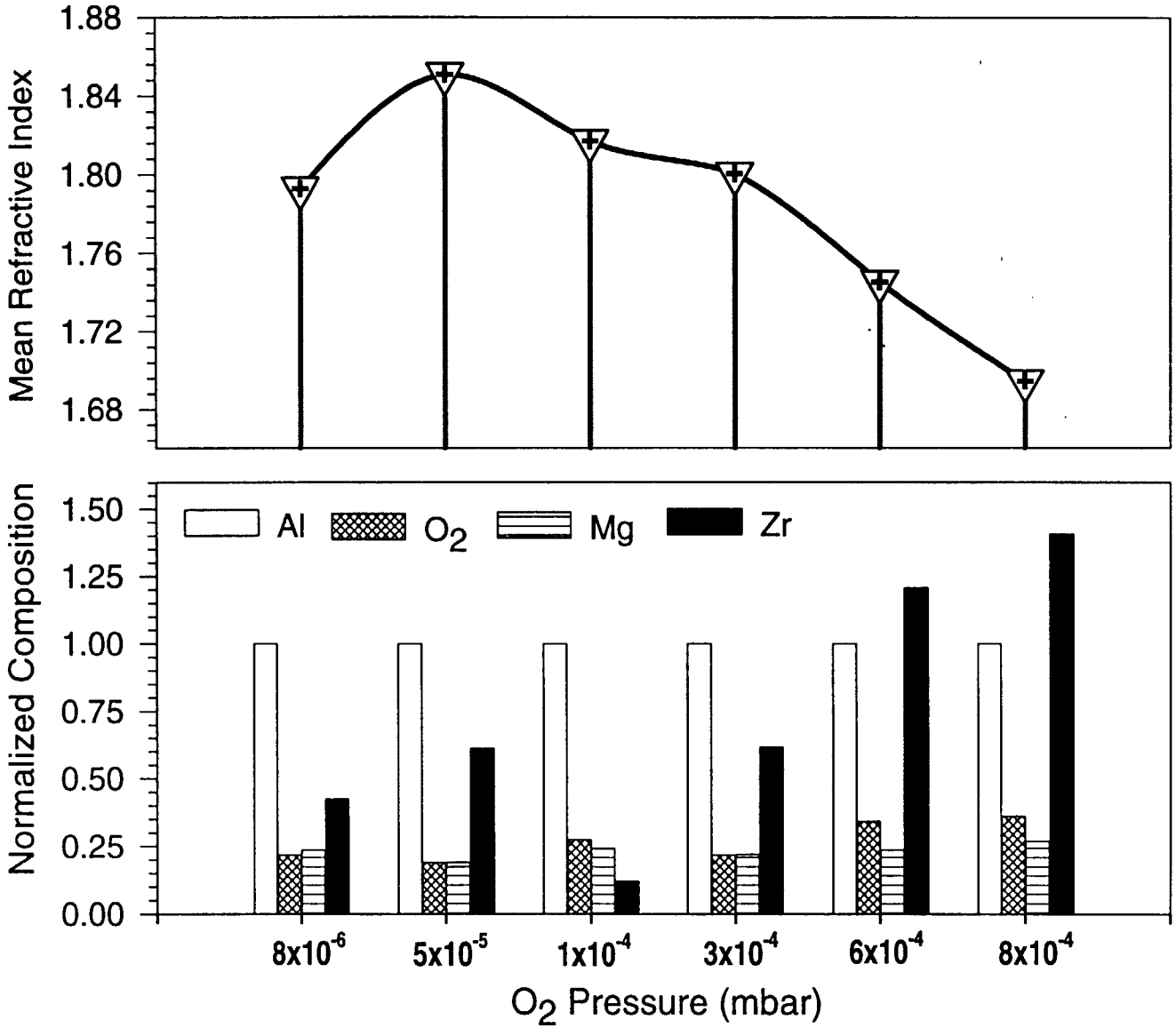
Mean Refractive Index
1.88
1.84
1.80
1.76
1.72
1.68
Normalized Composition
1.50
1.25
1.00
0.75
0.50
0.25
0.00
Al
O2
Mg
Zr
8x10-6
5x10-5
1x10-4
3x10-4
6x10-4
8x10-4
O2 Pressure (mbar)

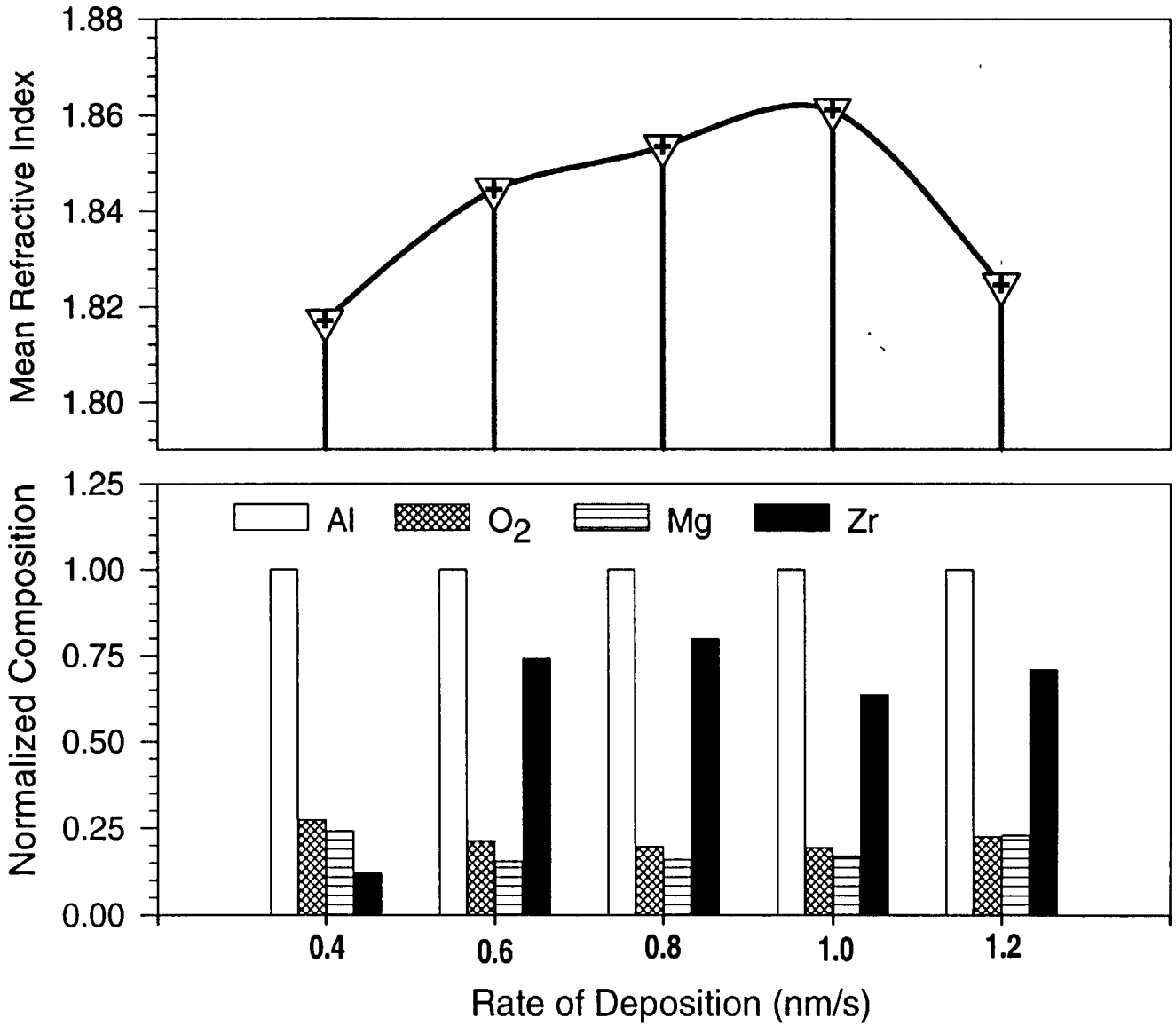
1.88
1.86
1.84
1.82
1.80
Mean Refractive Index
1.25
1.00
0.75
0.50
0.25
0.00
Normalized Composition
Al
O2
Mg
Zr
0.4
0.6
0.8
1.0
1.2
Rate of Deposition (nm/s)

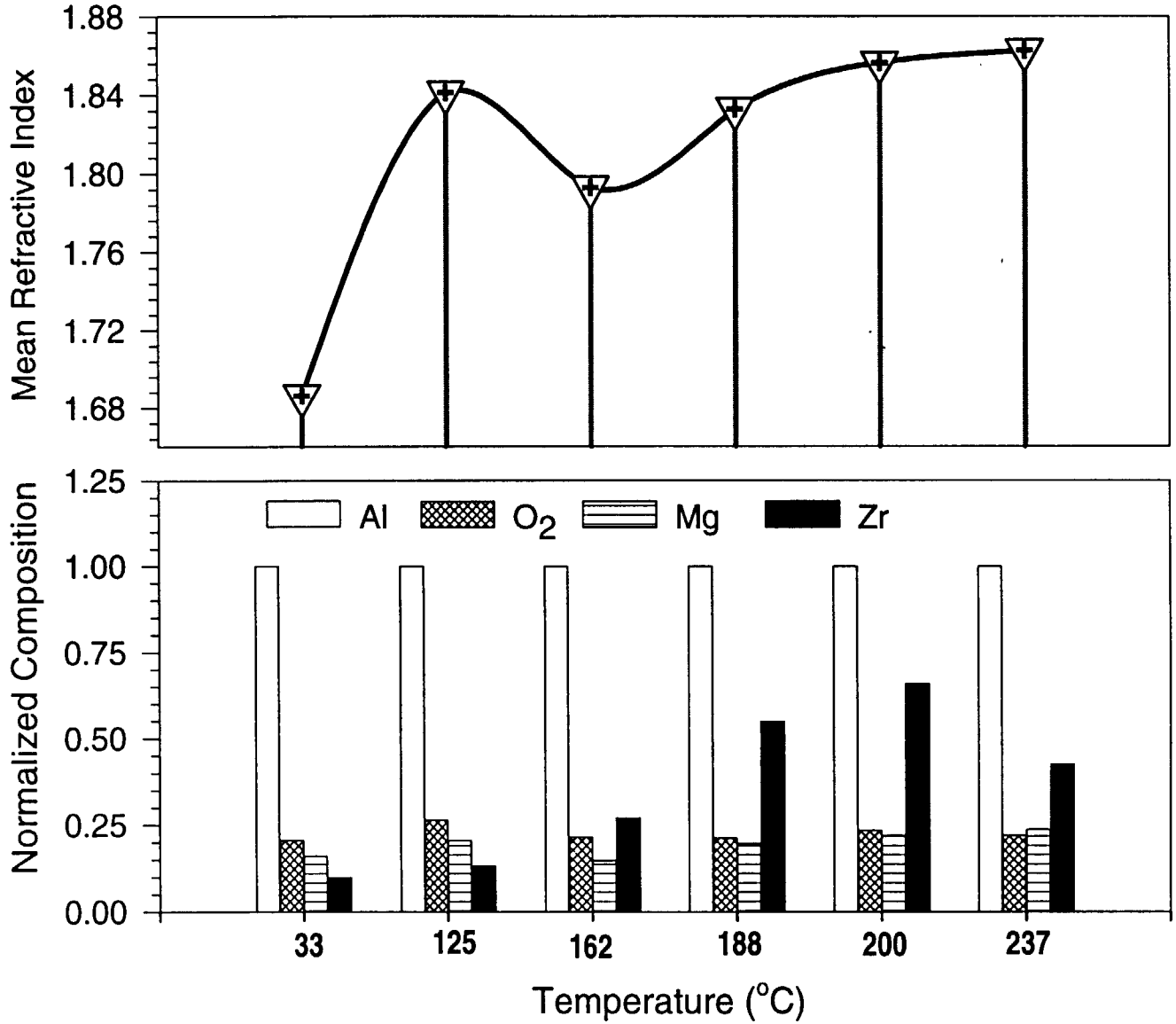
1.88
1.84
1.80
1.76
1.72
1.68
Mean Refractive Index
1.25
1.00
0.75
0.50
0.25
0.00
Normalized Composition
Al
O2
Mg
Zr
33
125
162
188
200
237
Temperature (°C)

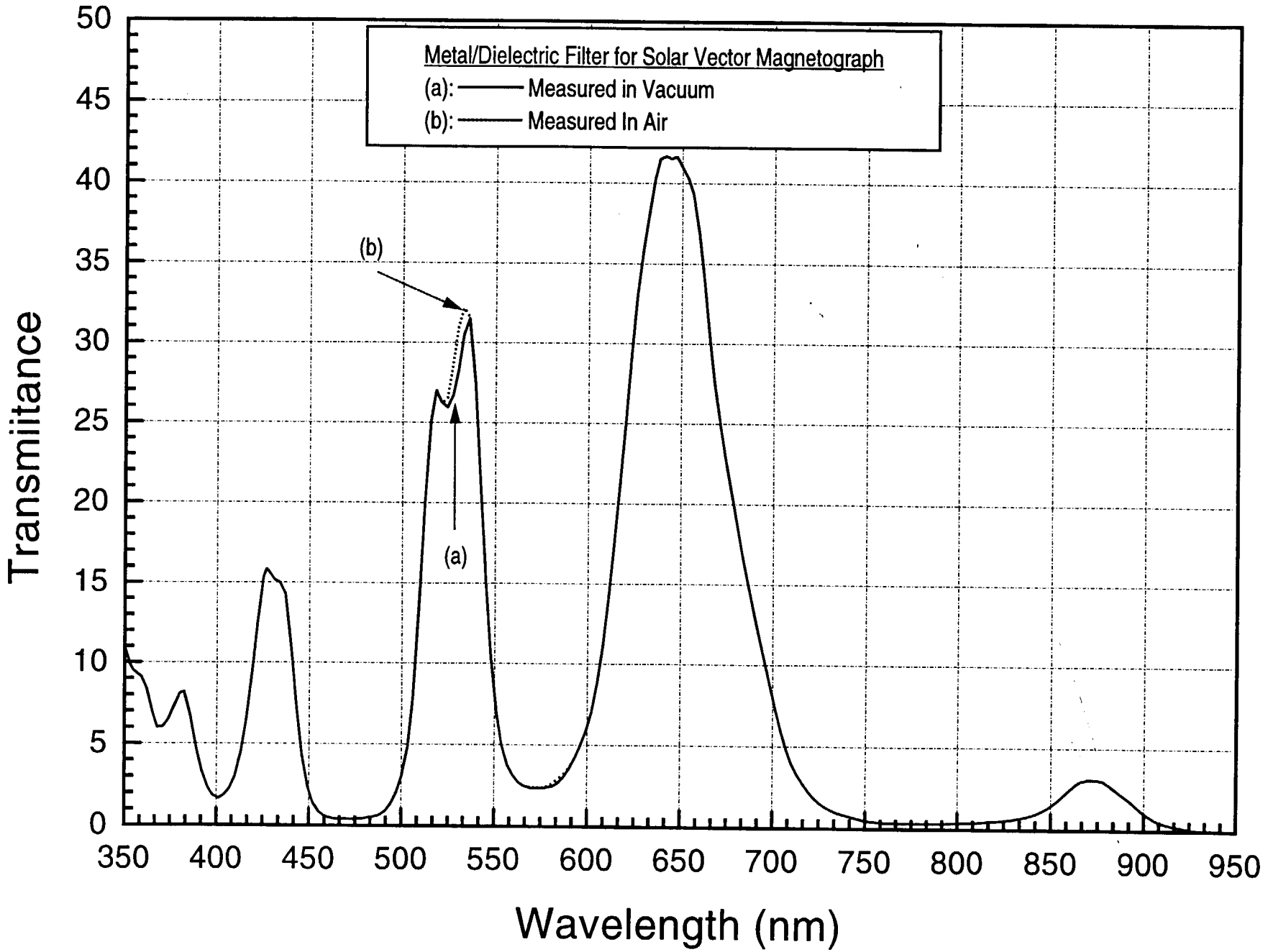
Metal/Dielectric Filter for Solar Vector Magnetograph
(a): Measured in Vacuum
(b): Measured In Air
(b)
(a)
Transmiitance
Wavelength (nm)
50
45
40
35
30
25
20
15
10
5
0
350
400
450
500
550
600
650
700
750
800
850
900
950

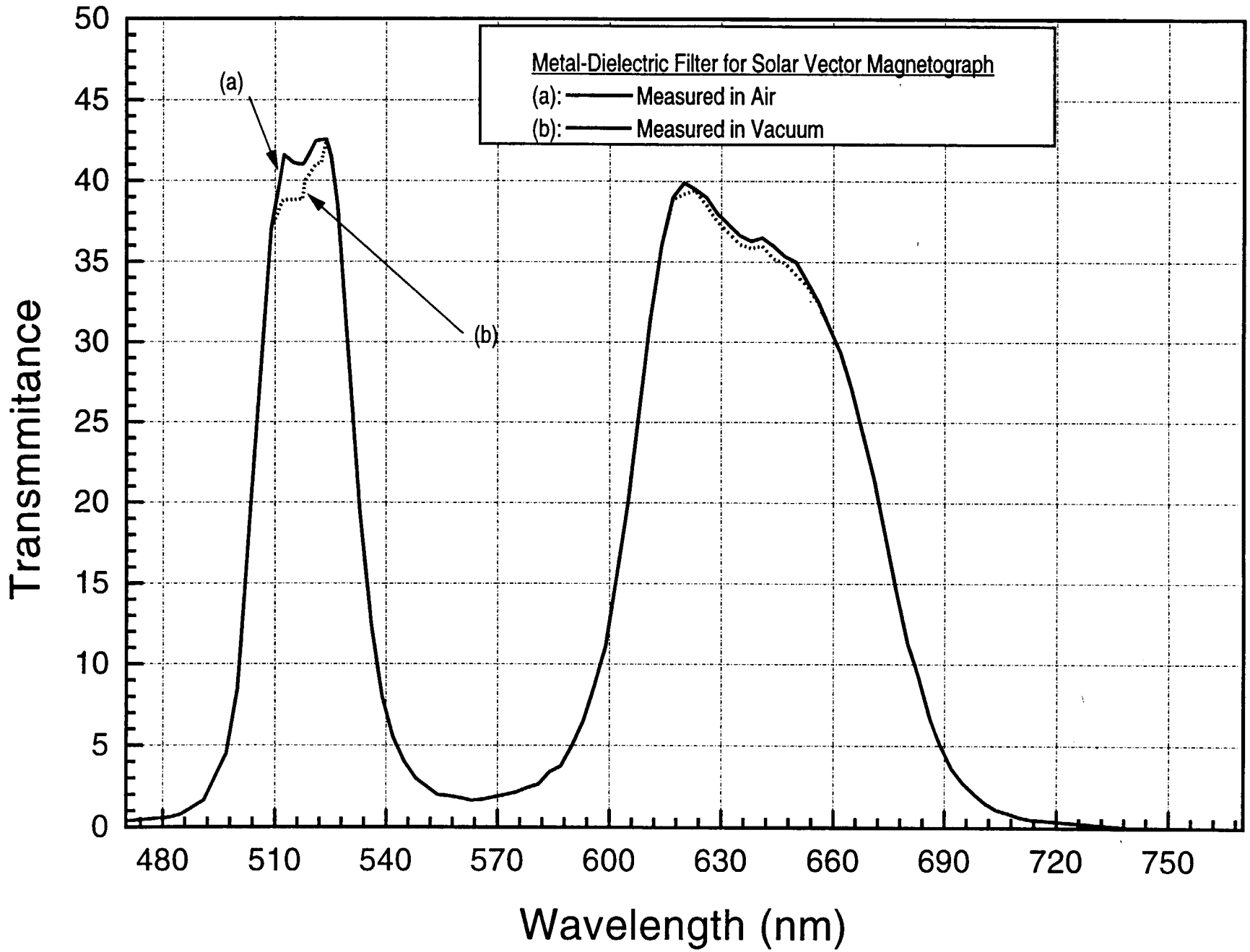
Metal-Dielectric Filter for Solar Vector Magnetograph
(a): Measured in Air
(b): Measured in Vacuum
(a)
(b)
Transmmitance
Wavelength (nm)
0
5
10
15
20
25
30
35
40
45
50
480
510
540
570
600
630
660
690
720
750